DOKUZ EYLÜL UNIVERSITY
GRADUATE SCHOOL OF NATURAL AND APPLIED SCIENCES

END POINT VIBRATION CONTROL OF FLEXIBLE SERIAL MANIPULATORS BY ACTIVE CABLE TENSION

by
Hayrettin ŞEN

August, 2023
İZMİR

END POINT VIBRATION CONTROL OF FLEXIBLE SERIAL MANIPULATORS BY ACTIVE CABLE TENSION

A Thesis Submitted to the
Graduate School of Natural and Applied Sciences of Dokuz Eylül University
In Partial Fulfillment of the Requirements for the Degree of Doctor of Philosophy in Department of Mechatronics Engineering

by
Hayrettin ŞEN

August, 2023
İZMİR

Ph.D. THESIS EXAMINATION RESULT FORM

We have read the thesis entitled "**END POINT VIBRATION CONTROL OF FLEXIBLE SERIAL MANIPULATORS BY ACTIVE CABLE TENSION**" completed by **HAYRETTİN ŞEN** under supervision of **ASST.PROF.DR. MURAT AKDAĞ** and we certify that in our opinion it is fully adequate, in scope and in quality, as a thesis for the degree of Doctor of Philosophy.

....

Asst. Prof. Dr. Murat AKDAĞ

Supervisor

....

Prof. Dr. Zeki KIRAL

Thesis Committee Member

....

Prof. Dr. Binnur GÖREN KIRAL

Thesis Committee Member

....

Prof. Dr. Hira KARAGÜLLE

Examining Committee Member

....

Assoc. Prof. Dr. Erkin GEZGİN

Examining Committee Member

Prof. Dr. Okan FISTIKOĞLU

Director

Graduate School of Natural and Applied Sciences

ACKNOWLEDGMENT

First of all, I would like to thank to my supervisor Assist. Prof. Dr. Murat AKDAĞ who helped me very much and taught me many valuable lessons, assisted me during my thesis and advised me whenever I needed guidance.

I would like to thank to my thesis committee members Prof. Dr. Zeki KIRAL and Prof. Dr. Binnur GÖREN KIRAL who made comments and gave ideas to solve some problems that I encountered during my thesis.

I am also thankful to Assoc. Prof. Dr. Şahin YAVUZ who helped me during the experiments and give guidance when I needed.

I also would like to thank the undergraduate student Ali DEMİR for helping me during the manufacturing process of experimental setup.

I would like to thank to my parents who raised and supported me until today.

And I would like to thank to my little and sweet daughter who gave me happiness and positive energy.

Finally, I am too much grateful to my wife for being too much patient and kind with me, helping and supporting me during the all steps of my study and to give happiness during my life.

Hayrettin ŞEN

END POINT VIBRATION CONTROL OF FLEXIBLE SERIAL MANIPULATORS BY ACTIVE CABLE TENSION

ABSTRACT

In this study, the effect of the time parameters of a 3^{rd} order polynomial S-curve on the endpoint vibrations of a flexible manipulator was investigated. The time parameters were defined in relation with the natural period of the flexible manipulator. The S-curve motion profile results were compared with the vibration results under the trapezoidal motion profiles. A finite element model of the flexible robot manipulator was created and the solution of the transient response under given velocity motion profile was calculated by using Newmark method. The finite element model was also established by using ANSYS and the obtained transient response results from ANSYS were compared with the results of Newmark calculation.

After this comparison the effect of the time parameters of three different types of S-curve motion profile on the vibrations of a flexible manipulator was investigated. These motion profiles were 3rd order polynomial S-curve velocity motion profile, harmonic sinusoidal motion profile and pure sinusoidal motion profiles. The effects of the time parameters on the transient response were observed by performing both finite element analyses and experiments. The sensitivity of vibration results to natural frequency measurement error of 4 percent was shown for the all motion profiles.

In the end, the finite element models of the flexible beam with cables were created and modal analysis were performed in ANSYS. The effect of both the presence of the cables and the initial tension on the cables on the natural frequency of the flexible manipulator were observed. The vibration results of the flexible manipulators with and without cable under the same velocity motion profiles were compared. Lastly, the closed loop control was performed, and the comparison of open and closed loop control results was made in terms of RMS values both experimentally and by using simulations.

Keywords: Vibration control, flexible manipulator, finite element analysis, active tension control

ESNEK SERİ ROBOTLARIN AKTİF KABLO GERGİSİ İLE UÇ NOKTA TİTREŞİM KONTROLÜ

ÖZ

Bu çalışmada, ilk olarak esnek manipülatörün doğal periyodu ile ilişkili 3. dereceden polinom S-eğrisi hız hareket profili zaman parametrelerinin esnek bir kirişin uç nokta titreşimlerine etkisi incelenmiştir. Zaman parametreleri, esnek manipülatörün doğal periyodu ile ilişkili olarak tanımlanmıştır. S-eğrisi hareket profili sonuçları, trapez hareket profilleri altındaki titreşim sonuçları ile karşılaştırılmıştır. Esnek robot manipülatörünün sonlu elemanlar modeli oluşturulmuş ve verilen hız hareket profili altındaki tepki çözümü Newmark yöntemi kullanılarak hesaplanmıştır. Ayrıca ANSYS kullanılarak sonlu eleman modeli kurulmuş ve ANSYS'den elde edilen geçici davranış sonuçları Newmark yöntemiyle elde edilen hesaplama sonuçları ile karşılaştırılmıştır.

Bu karşılaştırmadan sonra, üç farklı S-eğrisi hareket profili zaman parametresinin esnek bir manipülatörün titreşimleri üzerindeki etkisi de incelenmiştir. Bu hareket profilleri, 3. dereceden polinom S-eğrisi hız hareket profili, harmonik sinüzoidal hareket profili ve saf sinüzoidal hareket profilleridir. Zaman parametrelerinin geçici davranış üzerindeki etkileri hem sonlu eleman analizleri hem de deneyler yapılarak gözlemlendi. Titreşim sonuçlarının yüzde 4 doğal frekans ölçüm hatasına duyarlılığı da üç hareket profili için gösterilmiştir.

Son olarak kablolu esnek kirişin sonlu elemanlar modeli kurulmuş ve ANSYS'de modal analizi yapılmıştır. Esnek manipülatörün doğal frekansı üzerinde hem kabloların varlığının hem de kablolar üzerindeki ön gergi miktarının etkisi gözlemlendi. Aynı hız hareket profilleri altında kablolu ve kablolu olmayan titreşim sonuçları karşılaştırılmıştır. Son olarak kapalı çevrim kontrol gerçekleştirilmiş, açık ve kapalı çevrim kontrol sonuçlarının RMS değerleri açısından karşılaştırılması hem deneysel olarak hem de simülasyonlar kullanılarak yapılmıştır.

Anahtar kelimeler: Titreşim kontrolü, esnek manipülatör, sonlu elemanlar analizi, aktif gergi kontrolü

CONTENTS

Page

LIST OF FIGURES

Page

LIST OF TABLES

Page

LIST OF SYMBOLS

m_L	: Payload mass
m_{sen}	: Sensor mass
I_L	: Rotational inertia of payload
I_{sen}	: Rotational inertia of sensor
θ_2	: Instantaneous angular position of beam
t	: Time
L_2	: Length of the link
n_{e2}	: Number of finite elements
h_n	: Length of finite element-n
γ_n	: Instantaneous angle of orientation of finite element-n
$\mathbf{d}_{eln}$	: Displacement matrix of an element in local coordinates
$\mathbf{f}_{eln}$	: Force matrix of an element in local coordinates
$\mathbf{k}_{eln}$	: Stiffness matrix of an element in local coordinates
$\mathbf{m}_{eln}$	: Mass matrix of an element in local coordinates
A_n	: Cross section of finite element-n
x_n	: x axis of local cartesian coordinate
y_n	: y axis of local cartesian coordinate
u_{mn}	: Nodal displacement at Node-m in the x_n direction
v_{nm}	: Nodal displacement in the y_n direction
r_{mn}	: Flexural rotation of the cross section at Node-m
$F_{mnx'}$	: External forces at Node-m in the x_n
$F_{mny'}$	: External forces at Node-m in the y_n
T_{mn}	: External bending moment at Node-m
$q_{nx'}$	: distributed external loads in the x_n direction
$q_{ny'}$	: distributed external loads in the y_n direction
E_n	: Elastic modulus of of finite element-n
I_n	: Bending moment of inertia of the cross section
ρ_n	: Density
$\mathbf{d}_{egn}$	: Displacement matrix of an element in global coordinates
$\mathbf{f}_{egn}$	: Force matrix of an element in global coordinates

$\mathbf{k}_{egn}$	: Stiffness matrix of an element in global coordinates
$\mathbf{m}_{egn}$	: Mass matrix of an element in global coordinates
K_{m2}	: Rotational spring coefficient of motor
$\mathbf{m}_{s}$	: System mass matrix
$\mathbf{k}_{s}$	: System stiffness matrix
$\mathbf{c}_{s}$	: System damping matrix
$\mathbf{d}_{s}$	: System displacement matrix
$\mathbf{f}_{s}$	: System force matrix
η	: Coefficient of mass matrix for Rayleigh damping
β	: Coefficient of stiffness matrix for Rayleigh damping
T_n	: First natural period
Δt	: Time step
T_{acc}	: Acceleration time of the trapezoidal motion profile
T_{dec}	: Deceleration time of the trapezoidal motion profile
T_m	: Total motion time of a motion profile
D_{max}	: Total motion angle of a motion profile
$\mathbf{qt}_{m}$	: Trapezoidal motion profile vector
V_{max}	: Maximum velocity of a motion profile
A_{max}	: Maximum acceleration of a motion profile
T_i	: Time parameters of S-curve motion profiles (i=1,2,3,…7)
$\mathbf{qs}_{m}$	: 3^{rd} order polynomial S-curve motion profile vector
t1h	: Half of the fundamental natural period of the manipulator
J_{s_max}	: Maximum jerk value of polynomial S-curve motion profile
J_{hsin_max}	: Maximum jerk value of harmonic sinusoidal motion profile
J_{psin_max}	: Maximum jerk value of pure sinusoidal motion profile
$\mathbf{qhsin}_{m}$	: Harmonic sinusoidal motion profile vector
$\mathbf{qpsin}_{m}$	: Pure sinusoidal motion profile vector
Fax_{yield}	: Yield axial force
σ_{yield}	: Yield stress
A_{cable}	: Cross section area of cable
P_{crt}	: Critical buckling load
L_e	: Equivalent length of buckling critical load calculation

K_p	: Proportional control gain of closed loop control
K_d	: Derivative control gain of closed loop control
K_i	: Integral control gain of closed loop control
K_p	: Proportional control gain of closed loop control
K_p	: Proportional control gain of closed loop control
Kv	: Proportional control gain of for displacement feedback
Kvi	: Integral control gain of for displacement feedback

ABBREVIATIONS

FEM	: Finite element model
FE	: Finite element
DOF	: Degree of freedom
ODE	: Ordinary differential equation
RMS	: Root mean square

CHAPTER ONE

INTRODUCTION

1.1 Study Area

In its simplest form vibration can be considered the oscillation or repetitive motion of an object around an equilibrium position. Vibration control can be defined as the control or suppression of these oscillations or repetitive motions.

Vibration can cause several types of problems. These problems can be;

- Fatigue failure
- Structures like aircraft fuselage
- Machine components like crankshaft.
- Severe damages due to resonance
- Collapsing of bridges
- Damages in dynamic structures
- Loss of accuracy of work-piece due to vibration of machine tools.

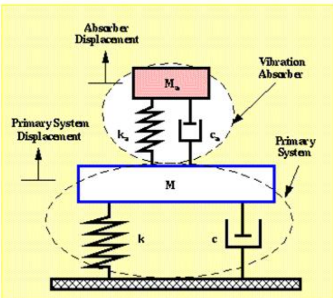

Figure 1.1 Passive vibration control of mass damper system

Vibration control can be categories in two groups as passive and active vibration control. In passive control, suppression of vibrations can be achieved by limiting the ability of vibrations to be coupled to the item to be isolated. This can be done using a mechanical modification that disperse the energy of vibration before it gets to the item to be isolated as shown in Figure 1.1. The new attached mass can cause passive control.

Serial manipulators are commonly used in industry for too many purposes such as pick and place, welding, path following applications etc. During their motion or working process the end effector vibration of the serial manipulator should be controlled. This control is achieved in a passive way by increasing the rigidity of the arms of the manipulators in industry. The weight of the arms is also increased via this rigidity. However, the amount of payload the robot can carry decrease. For this reason, the low weight serial flexible robots can be used to perform these types of tasks. These type of flexible manipulators were defined as manipulators which have low weight or large dimensions in the study (Gao, Wang, Zhao, & Xiao, 2012). In many literature reviews (Benosman & Le Vey, 2004; Dwivedy & Eberhard, 2006; Sayahkarajy, Mohamed, & Mohd Faudzi, 2016; Subedi, Tyapin, & Hovland, 2020) includes the design, dynamic analyses and passive and active vibration control studies of flexible robots. Therefore, these types of robots can be actuated with low power motors due to their low weight. However, there is vibration problem of these type of manipulators.

However, the passive vibration control of the serial manipulators can be performed by giving the appropriate velocity input to the servo motor which rotates the flexible arm. This velocity input aims only to rotate the arm, not to control the vibrations. The structure of the input velocity profile suppresses the residual vibration of the flexible arm. Passive vibration control can be used pick and place applications. During the motion the vibration control does not exist.

A residual vibration problem of a flexible link manipulator driven by a cycloidal motion profile were studied by Ankaralı and Diken. It was found that at certain frequencies of the rise time of the motion profile causes the zero-residual vibration (Ankarali & Diken, 1997). An experimental study were performed on a rotating flexible aluminum arm by Diken and Alghamdi (Diken & Alghamdi, 2003) to verify the simulation study results of Ankaralı (Ankarali & Diken, 1997).

Trapezoidal velocity motion profile is the basic motion profile which is used to actuate a manipulator. Trapezoidal velocity profiles consist of three-time parameters which are acceleration time, deceleration time and constant velocity time. Selection of these time parameters are crucial for elimination of end point vibrations of a flexible manipulator or to keep them at a certain level. Some studies (Malgaca, Yavuz, Akdağ, & Karagülle, 2016; Yavuz, Malgaca, & Karagülle, 2016) proved that selection of the trapezoidal motion profile time parameters which are related with the natural period of the one degree of freedom flexible manipulator, suppress the residual vibrations. The same approach was also used for two degrees of freedom flexible manipulator and the residual vibrations were reduced in the study (Karagülle, Malgaca, Dirilmiş, Akdağ, & Yavuz, 2017). In these studies (Karagülle et al., 2017; Malgaca et al., 2016; Yavuz et al., 2016) when the deceleration time of trapezoidal motion profile was selected as integer multiples of first natural period of the manipulator, the residual vibrations were suppressed.

In the literature, different velocity profiles which have smoother acceleration changes than trapezoidal velocity motion profiles were suggested and used to actuate a motor or dynamic system. The first proposed the 3rd order S-curve motion profile which has seven-time segment by Castain and Paul (Castain & Paul, 1984) was used also in practice (C. Liu & Chen, 2018; S. Liu, 2002; T.-C. Lu & Chen, 2016; Mu, Zhou, Yan, & Han, 2008), since it has moderate complexity to use and enables the motion to happen in minimum amount of time with limited jerk.

Higher order motion profiles were also used for required high precision due to the continuous jerk profile (Boryga & Graboś, 2009). The 4th order S-curve motion profile that has fifteen time segment were selected and used in studies (Boryga & Graboś, 2009; Lambrechts, Boerlage, & Steinbuch, 2005). An algorithmic study was also proposed by Nguyen et. al. for designing a motion profile which has desired order (Nguyen, Ng, & Chen, 2008). In their study, a seven-segment velocity profile which has harmonic jerk model was also designed and it was represented that while the higher order motion profiles caused less position error, the minimum position error occurs when the velocity profile with the harmonic jerk model was used.

A dimensionless ramp up time of a 3rd order S-curve motion profile was designed using a reference trapezoidal velocity motion profile acceleration time and the natural period of a lightly-damped system in the study of Meckl and Arestides (Meckl & Arestides, 1998). In the simulation studies it was obtained that the proposed new 3rd order S-curve motion profile caused less residual vibration results than both reference trapezoidal velocity motion profile and 3rd order S-curve motion profile which has a ratio of 1/6 between ramp up time and acceleration time.

In the study of Li et al. (HZ Li, Gong, Lin, & Lippa, 2006) a three-segment motion profile which has a sinusoidal acceleration function was proposed and experimental vibration results of a linear motion under both the given trapezoidal velocity profile and the proposed motion profile were discussed. They also proposed (Huaizhong Li, Le, Gong, & Lin, 2009) a seven-segment motion profile which has a sinusoidal jerk profile. The experimental results of point to point linear motion under the given input trapezoidal velocity motion profile, 3rd order S-curve motion profile and proposed seven-segment motion profile were discussed in terms of residual vibrations.

Byeogjin Kim et al. (B. Kim, Yoo, & Chung, 2017) studied the residual vibrations of an undamped system under motion profiles which have trigonometric and trapezoidal acceleration profiles. In their study the motion profiles were designed by predefined time parameter values. It was observed that the zero vibration conditions were obtained if the time parameters were selected as integer-multiples of first natural period for the trapezoidal acceleration profiles and half-integer multiples of first natural period for trigonometric profiles.

The effect of the time parameters of 3rd order polynomial S-curve and trapezoidal motion profiles on transient and residual vibrations of a flexible manipulator were investigated (Akdağ & Şen, 2021). Finite element model of manipulator was created, and numerical calculations were done by using Newmark method.

Fang et al. (Fang et al., 2019) proposed an S-curve motion profile which has fifteen time segment and sigmoid jerk profile. Experimental residual vibration results of six-

DOF manipulator for point-to-point motion were shown and it was observed that proposed motion profile gave better result for end-point vibrations than both the trapezoidal velocity motion profile and 7th order S-curve motion profile.

Input shaping method is an open loop control technique which creates the input pulses by using system's natural frequency and damping ratio. Input shaping method (Hillsley & Yurkovich, 1993; Tzes & Yurkovich, 1993) was used to suppress the residual vibration of flexible manipulator. There are also many studies made investigation about the input-shaping method to shape the motion profile by using preprocessing filter (Ha & Lee, 2017; J. Kim & Croft, 2018; Mohamed & Tokhi, 2004; Singer & Seering, 1990; Thomsen, Søe-Knudsen, Balling, & Zhang, 2021). Singer et al. designed an impulse shaping technique which converts the reference input to a new impulse sets which do not trigger system at its resonance. In order to decrease the effect of the original input on the vibrations, a part of the input was delayed by half of the damped natural period of system (Singer & Seering, 1990).

As mentioned above there are many studies which was made investigation for the elimination the residual and transient vibrations of the flexible systems. The mentioned studies are used passive vibration control or open loop control. The other vibration control method is the active vibration control.

In the active vibration control one actuator should be used to suppress or control the vibrations. This actuator can be piezo electric actuators or a servo motor which rotates the flexible arm. Some studies were used the actuation motor as control actuator. In these studies generally strain feedback was used to control the residual vibrations (Bernzen, 1999; Ilman, Yavuz, Karagülle, & Uysal, 2022; Jnifene, 2007; Jnifene & Andrews, 2005; Qiu, Li, & Zhang, 2019; Yatim & Mat Darus, 2014). In the study of Bernzen vibration control of a single link flexible manipulator was studied by using a DC motor with a gear ratio of 66. He implemented a linear PI controller to system by using an angular velocity feedback (Bernzen, 1999).

There are also many studies which use the piezoelectric actuator as a control actuator to control the end point vibrations of the flexible manipulators (Dubay, Hassan, Li, & Charest, 2014; Hassan, Dubay, Li, & Wang, 2007; E. Lu, Li, Yang, Wang, & Liu, 2018; Tzou, 1989; Wei, Qiu, Han, & Wang, 2010). In the study of Dubay R. et al vibration control of a single link flexible manipulator was studied by using the piezoelectric actuators. They used an advanced model predictive controller to eliminate the end tip vibrations with strain feedback (Dubay et al., 2014).

Another type of active vibration control method is to control the vibrations by active cable tension. These types of controllers were used in the literature to control either vibration of cable stated bridges or truss structures. The study of Preumont et al. the active tendon control of large trusses and bridges was performed. In their study piezoelectric stack actuators were used (Achkire, Bossens, & Preumont, 1998; Achkire & Preumont, 1996; Bossens & Preumont, 2001; André Preumont & Achkire, 1997; André Preumont, Achkire, & Bossens, 2000; André Preumont & Bossens, 2000; Andre Preumont, Voltan, Sangiovanni, Mokrani, & Alaluf, 2016). In the study of Warnitchai et al. the vibration of one fixed support beam was studied (Warnitchai, Fujino, Pacheco, & Agret, 1993). They also used piezoelectric stack actuator.

This method was also used to control the vibration of the membrane antenna structure by Liu et al. (X. Liu, Zhang, Lv, Peng, & Cai, 2018). Rodellar studied on the vibration control of the cable-stayed bridges under the seismic excitation (Rodellar, Mañosa, & Monroy, 2002).

In this thesis the passive and active vibration control were studied. Four different types of velocity motion profiles were used to achieve the passive vibration control. The effect of their time parameters was investigated on the vibrations of the flexible manipulator. This investigation was done both in simulations and experimentally. The active vibration control of flexible manipulator was also studied by using the active cable tensions. The finite element model of a flexible beam was created in ANSYS and open loop and closed loop control simulations were performed. The experimental setup was produced, and the open and closed loop control were studied on this experimental setup.

1.2 Purpose and Scope

In this thesis the passive and active vibration control were studied. Four different types of velocity motion profiles were used to achieve the passive vibration control. The used velocity motion profiles were also used in the literature to control vibration of structures. The used velocity motion profiles trapezoidal velocity motion profiles, 3rd order polynomial, harmonic sinus and pure sinus S-curve motion profiles. The main idea to obtain the less vibration amplitudes during and after the motion. Design of these motion profiles were performed which cause the minimum vibration amplitudes. The effect of time parameters of these motion profiles was also investigated on the vibration amplitudes. This investigation was done both in simulations and experimentally. Simulations were performed in ANSYS. Single link flexible manipulator was used during the study. The effects of the parameters of these three velocity motion profiles on the vibrations of flexible manipulators have been investigated comparatively for the first time.

The active vibration control of flexible manipulator was also studied. The active vibration control was studied on a single link flexible manipulator by using the active cable tensions. This control method was used to control the vibration of cable-stayed bridges and truss structures. In this thesis this method was used on a more flexible structure. The effect of both presence of the cables and initial tension on the cables on the natural frequency of the flexible manipulator were observed. The vibration results of with and without cable condition under the same velocity motion profiles were compared. The finite element model of a flexible beam was created in ANSYS and open loop and closed loop control simulations were performed. An experimental setup was produced according to simulation results. The open and closed loop control were studied on this experimental setup. The closed loop control results were compared with the open loop ones in terms of RMS values both experimentally and by using simulations.

CHAPTER TWO
S-CURVE MOTION PROFILE DESIGN FOR VIBRATION CONTROL OF SINGLE LINK FLEXIBLE MANIPULATOR

2.1 Methodology

In this chapter, passive vibration control was achieved by designing 3rd order S-curve velocity motion profiles. The effect of the time parameters of this motion profile which were defined in relation with the natural period of the manipulator on endpoint vibrations of a flexible beam were investigated (Akdağ & Şen, 2021). The vibration results of the S-curve motion profiles were compared to the vibration results under trapezoidal motion profiles. The finite element model of the manipulator was created in both MATLAB and ANSYS. The transient response of the manipulator under the motion profiles was calculated by the Newmark method in MATLAB. The obtained results from Newmark method were compared with the ANSYS results.

2.2 Finite Element Modeling and Analyses by using MATLAB Code and ANSYS

2.2.1 FE (Finite Element) Modeling

A code was written in MATLAB based on the finite element method (FEM) (Bathe, 2014). Figure 2.1 (a) shows the one link manipulator presented in this study, as modeled in MATLAB. The OB-beam was designated as Member-2. Member-2 and Member-1 (fixed frame) were connected at point O using a revolute joint. The mass of the motor, which is used to rotate Member-2, is applied on the frame at point O. The payload and sensor, which are placed at point B and C, have a translational inertia of m_L and m_{sen} and rotational inertia of I_L and I_{sen} respectively.

The instantaneous angular position of Member-2 is $\theta_2(t)$. L_2 represent the link length of OB. A global Cartesian coordinate system was used with O is the origin and x, y and z as the main axes.

Figure 2.1(b) depicts the FE model of the link. n_{e2} designates the number of finite elements. Figure 2.1(b) gives a simplified illustration in which n_{e2} was chosen to be 3. The same procedure can be applied to create models with a larger of finite elements. The code was written in a generalized form, such that any desired n_{e2} can be implemented (Karagülle et al., 2017; Malgaca et al., 2016).

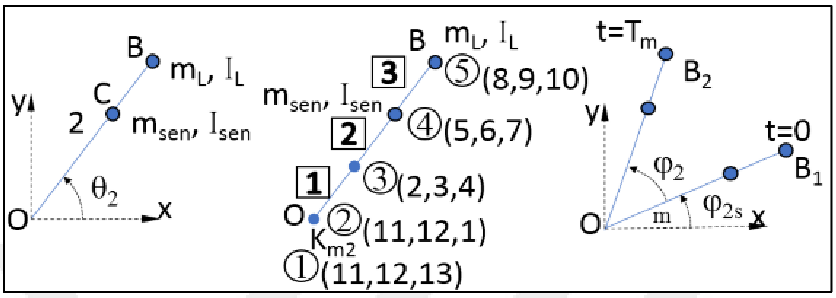

(a) (b) (c)

Figure 2.1 (a) Schematic model (b) Elements and nodes of model (c) Start and end positions

In the Figure 2.1(b) circles are used to designate node numbers, while squares are used to designate numbers of the finite elements. A plane frame analysis, in which each node has two translational and one rotational DOF, was performed. The identification numbers of DOFs for each node are indicated in parentheses next to the corresponding node number. For instance, FE-3 is defined by nodes 4 and 5. The DOFs for Node-4 are d_{s5}, d_{s6}, and d_{s7}. The local Cartesian coordinate system was considered for FE-3, in which the axes are designated as x_3, y_3 and z_3. The local coordinate system is rotated in such a way that the origin is located at Node-4 and x_3 axis is pointed towards Node-5. Due plane frame analysis, the z axes of the global and local coordinate systems are always parallel. The translational DOFs of Node-4 are d_{s5} and d_{s6} in x and y directions, respectively, while the rotational DOF at this node is r_{s7} and $d_{s7}=h_3 r_{s7}$, where h_3 designates the length of FE-3. The instantaneous angle of orientation for x_3 is $\gamma_3= \theta_2$ (Karagülle et al., 2017; Malgaca et al., 2016). Table 2.1 summarizes the FE model of the link and its defining parameters.

The FE analysis theory has been explained in detail elsewhere (Bathe, 2014). Eq. (2.1) gives the displacement ($\mathbf{d}_{eln}$) and mass ($\mathbf{m}_{eln}$) matrices, Eq. (2.2) gives the stiffness ($\mathbf{k}_{eln}$) matrix, and Eq. (2.3) gives the force ($\mathbf{f}_{eln}$) matrix of a finite element in local coordinates, where j and k are the node numbers at the origin and the far end of the given FE (Bathe, 2014; Karagülle et al., 2017; Malgaca et al., 2016).

Table 2.1 FE parameters of Member-2

FE-	Nodes	Length	γ_n	Id. numbers for DOFs at nodes
1	2,3	L_2/n_{e2}	θ_2	11,12,1,2,3,4
2	3,4	L_2/n_{e2}	θ_2	2,3,4,5,6,7
3	4,5	L_2/n_{e2}	θ_2	5,6,7,8,9,10

$$\mathbf{d}_{eln} = \begin{Bmatrix} u_{jn} \\ v_{jn} \\ h_n r_{jn} \\ u_{kn} \\ v_{kn} \\ h_n r_{kn} \end{Bmatrix} \mathbf{m}_{eln} = \frac{\rho_n A_n h_n}{420} \begin{bmatrix} 140 & 0 & 0 & 70 & 0 & 0 \\ 0 & 156 & 22h_n & 0 & 54 & -13h_n \\ 0 & 22h_n & 4h_n^2 & 0 & 13h_n & -3h_n^2 \\ 70 & 0 & 0 & 140 & 0 & 0 \\ 0 & 54 & 13h_n & 0 & 156 & -22h_n \\ 0 & -13h_n & -3h_n^2 & 0 & -22h_n & 4h_n^2 \end{bmatrix} \tag{2.1}$$

$$\mathbf{k}_{eln} = \begin{bmatrix} \frac{A_nE_n}{h_n} & 0 & 0 & \frac{-A_nE_n}{h_n} & 0 & 0 \\ 0 & \frac{12E_nI_n}{h_n^3} & \frac{6E_nI_n}{h_n^2} & 0 & \frac{-12E_nI_n}{h_n^3} & \frac{6E_nI_n}{h_n^2} \\ 0 & \frac{6E_nI_n}{h_n^2} & \frac{4E_nI_n}{h_n} & 0 & \frac{-6E_nI_n}{h_n^2} & \frac{2E_nI_n}{h_n} \\ \frac{-A_nE_n}{h_n} & 0 & 0 & \frac{A_nE_n}{h_n} & 0 & 0 \\ 0 & \frac{-12E_nI_n}{h_n^3} & \frac{-6E_nI_n}{h_n^2} & 0 & \frac{12E_nI_n}{h_n^3} & \frac{-6E_nI_n}{h_n^2} \\ 0 & \frac{6E_nI_n}{h_n^2} & \frac{2E_nI_n}{h_n} & 0 & \frac{-6E_nI_n}{h_n^2} & \frac{4E_nI_n}{h_n} \end{bmatrix} \tag{2.2}$$

$$\mathbf{f}_{eln} = \begin{Bmatrix} F_{jnx'} + q_{nx'}\dfrac{h_n}{2} \\ F_{jny'} + q_{ny'}\dfrac{h_n}{2} \\ T_{jn} + q_{ny'}\dfrac{h_n^2}{12} \\ F_{knx'} + q_{nx'}\dfrac{h_n}{2} \\ F_{kny'} + q_{ny'}\dfrac{h_n}{2} \\ T_{kn} + q_{ny'}\dfrac{h_n^2}{12} \end{Bmatrix} \tag{2.3}$$

The parameters used in Eq (2.1) to Eq. (2.3) are explained below:

h_n – the length of the n^{th} FE

A_n – the cross-sectional area of the link

E_n – elastic modulus

I_n – moment of inertia

ρ_n – density

u_{mn} – the translational DOF in the local x direction of Node-m

v_{mn} – the translational DOF in the local y direction of Node-m

r_{mn} – the rotational DOF in the local z direction of Node-m

$F_{mnx'}$ – the external force in the local x direction of Node-m

$F_{mny'}$ – the external force in the local y direction of Node-m

T_{mn} – the external bending moment in the local z direction of Node-m

$q_{nx'}$ – the external distributed load in the local x direction of FE-n

$q_{ny'}$ – the external distributed load in the local y direction of FE-n

Eq. (2.4) shows the calculation in global coordinates of the displacement, stiffness, force and mass matrices (Bathe, 2014; Karagülle et al., 2017; Malgaca et al., 2016).

$$\begin{gathered} \mathbf{d}_{egn} = \mathbf{T}_n\mathbf{d}_{eln},\ \mathbf{k}_{egn} = \mathbf{T}_n^T\mathbf{k}_{eln}\mathbf{T}_n \\ \mathbf{f}_{egn} = \mathbf{T}_n\mathbf{f}_{eln},\ \mathbf{m}_{egn} = \mathbf{T}_n^T\mathbf{m}_{eln}\mathbf{T}_n \end{gathered} \tag{2.4}$$

In this equation, $\mathbf{T}_n$ and $\mathbf{T}_n^T$ are the transformation matrix and its transpose. Eq. (2.5) gives the transformation matrix.

$$\mathbf{T}_n = \begin{bmatrix} c_n & s_n & 0 & 0 & 0 & 0 \\ -s_n & c_n & 0 & 0 & 0 & 0 \\ 0 & 0 & 1 & 0 & 0 & 0 \\ 0 & 0 & 0 & c_n & s_n & 0 \\ 0 & 0 & 0 & -s_n & c_n & 0 \\ 0 & 0 & 0 & 0 & 0 & 1 \end{bmatrix} \tag{2.5}$$
$$c_n = \cos\gamma_n,\ s_n = \sin\gamma_n$$

For the example presented in Figure 2.1 (b) nodes 1 and 2 are coincident, however, they have different rotational DOF because of the revolute joint located at point O. A rotational spring (K_{m2}) placed between nodes 1 and 2 is used to model the motor. Masses used to represent the sensor and the payload are applied at nodes 4 and 5 respectively. Since Node-1 is fixed, its DOFs are equal to zero. The motor provides the torque required to resist rotation (Karagülle et al., 2017; Malgaca et al., 2016). The mathematical model of the flexible link is given in Eq. (2.6).

$$\mathbf{m}_s\ddot{\mathbf{d}}_s + \mathbf{c}_s\dot{\mathbf{d}}_s + \mathbf{k}_s\mathbf{d}_s = \mathbf{f}_s \tag{2.6}$$

The mass ($\mathbf{m}_s$), stiffness ($\mathbf{k}_s$) and damping ($\mathbf{c}_s$) matrices are 10x10 for the example shown in Figure 2.1. The force ($\mathbf{f}_s$) and displacement ($\mathbf{d}_s$) matrices are 10x1 for the same example. For instance, the translational DOF in the x direction of Node-4 is $\mathbf{d}_s(5,1)=d_{s5}$.

The stiffness and mass matrices of the flexible link are obtained by assembling the local FE matrices, which have sizes 6x6. An example of this assembly procedure is given in Eq. (2.7).

$$\begin{aligned} \mathbf{k}_s(6,5) &= \mathbf{k}_{eg2}(5,4) + \mathbf{k}_{eg3}(2,1) \\ \mathbf{m}_s(6,5) &= \mathbf{m}_{eg2}(5,4) + \mathbf{m}_{eg3}(2,1) \end{aligned} \tag{2.7}$$

The combination of the value of $\mathbf{k_s}(6,5)$ or $\mathbf{m_s}(6,5)$ matrix exist in FE-2 and FE-3 as seen in Table 2.1. When the kinetic energy of the sensor and payload are taken into consideration, mass (m_L, m_{sen}) and inertia (I_L, I_{sen}) values should be added to mass matrix as expressed in Eq. (2.8) and Eq. (2.9). When the potential energy of the system is considered, K_{m2} was added to the system stiffness matrix as shown in Eq. (2.10).

$$\begin{aligned} \mathbf{m}_s(5,5) &= \mathbf{m}_{eg2}(4,4) + m_{sen} \\ \mathbf{m}_s(6,6) &= \mathbf{m}_{eg2}(5,5) + m_{sen} \\ \mathbf{m}_s(7,7) &= \mathbf{m}_{eg2}(6,6) + I_{sen} \end{aligned} \tag{2.8}$$

$$\begin{aligned} \mathbf{m}_s(8,8) &= \mathbf{m}_{eg3}(4,4) + m_L \\ \mathbf{m}_s(9,9) &= \mathbf{m}_{eg3}(5,5) + m_L \\ \mathbf{m}_s(10,10) &= \mathbf{m}_{eg3}(6,6) + I_L \end{aligned} \tag{2.9}$$

$$\mathbf{k}_s(1,1) = \mathbf{k}_{eg2}(3,3) + K_{m2} \tag{2.10}$$

The damping matrix of the system was calculated by using Rayleigh damping coefficients as given in Eq. (2.11),

$$\mathbf{c}_s = \eta \mathbf{m}_s + \beta \mathbf{k}_s \tag{2.11}$$

where, η and β are the damping coefficients of damping matrix (W. T. Thomson, 1988).

2.2.2 Calculation of Newmark Method

The Newmark method (Newmark, 1959) was used for the calculation of the transient response of the manipulator under the velocity motion profiles. A fixed time step (Δt), was chosen for the calculations as $\Delta t<(T_n/20)$, where T_n is the first natural period (Karagülle et al., 2017). The solution at the next time step was calculated using numerical integration based on the results of the previous time step. Assuming $\mathbf{m_n}$, $\mathbf{c_n}$, $\mathbf{k_n}$, $\mathbf{d_n}$, and $\mathbf{f_n}$ be the mass, damping, stiffness, nodal displacement and nodal force matrices at the time step t_n, then solution using the Newmark method is shown in Eq. (2.12), Eq. (2.13) and Eq. (2.14). (Karagülle et al., 2017),

$$\begin{aligned}\left[a_0\mathbf{m}_n + a_1\mathbf{c}_n + \mathbf{k}_n\right]\mathbf{d}_{n+1} &= \mathbf{f}_n + \mathbf{m}_n\left[a_0\mathbf{d}_n + a_2\dot{\mathbf{d}}_n + a_3\ddot{\mathbf{d}}_n\right] \\ &+ c_n\left[a_1\mathbf{d}_n + a_4\dot{\mathbf{d}}_n + a_5\ddot{\mathbf{d}}_n\right]\end{aligned} \tag{2.12}$$

$$\ddot{\mathbf{d}}_{n+1} = a_0\left[\mathbf{d}_{n+1} - \mathbf{d}_n\right] - a_2\dot{\mathbf{d}}_n - a_3\ddot{\mathbf{d}}_n \tag{2.13}$$

$$\dot{\mathbf{d}}_{n+1} = \dot{\mathbf{d}}_n + a_6\ddot{\mathbf{d}}_n + a_7\ddot{\mathbf{d}}_{n+1} \tag{2.14}$$

$$\begin{gathered} a_0 = \frac{1}{\alpha\Delta t^2},\ a_1 = \frac{\delta}{\alpha\Delta t},\ a_2 = \frac{1}{\alpha\Delta t} \\ a_3 = \frac{1}{2\alpha} - 1,\ a_4 = \frac{\delta}{\alpha} - 1,\ a_5 = \frac{\Delta t}{2}\left(\frac{\delta}{\alpha} - 2\right) \\ a_6 = \Delta t\left(1-\delta\right),\ a_7 = \delta\Delta t \\ \alpha = \frac{1}{4}\left(1+\gamma\right)^2,\ \delta = \frac{1}{2} + \gamma \end{gathered} \tag{2.15}$$

where the coefficients from a_0 to a_7 are given in Eq. (2.15).

2.2.3 Modeling the Manipulator by using ANSYS

The FE model of the flexible beam was created in ANSYS. BEAM188 element type was used to model the flexible beam. BEAM188 element has two nodes and each node has 6 degree of freedoms. The transient response of the beam under a motion profile was also calculated in ANSYS using transient structural analysis. Two-point masses were added on the manipulator as payload and accelerometer mass. The modeled flexible manipulator is shown in Figure 2.2. The properties of the flexible link used in the numerical model are given in Table 2.2.

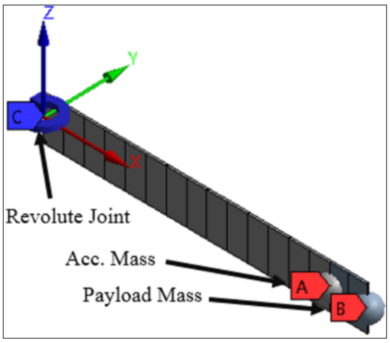

Figure 2.2 The established FE model in ANSYS

Table 2.2 FE model parameters

Elastic modulus	$2.1\text{x}10^{11}$ Pa
Poisson ratio	0.3
Density	7800 kg/m^3
Accelerometer mass	54 gr
Inertia of the accelerometer	$9.18450\text{x}10^{-6}$ kgm^2
Payload mass	130.69 gr
Inertia of payload	$1.49564\text{x}10^{-5}$ kgm^2
Cross section	1.95x40.6 mm^2
Beam length (L_2)	300 mm
Acc. Position from the origin	266 mm
Rayleigh damping coefficients	η=0 and β=$2\text{x}10^{-4}$
Newmark amp. decaying factor	γ =0.005
Motor rotational spring constant	K_{m2}=16000 Nm/rad
Number of finite elements	ne2=150
Time step	Δt=0.005 s

2.3 Trapezoidal and 3rd Order S-Curve Motion Profile Design

The design of the trapezoidal velocity profile for the desired motion angle and motion time parameters which are T_{acc}, T_{cons} and T_{dec}, is shown in Figure 2.3(a). The acceleration, velocity and displacement are given in equations from Eq. (2.17) to Eq. (2.25) Total motion time (T_m= T_{acc}+T_{cons}+T_{dec}), total motion angle (D_{max}) and time parameters (T_{acc}, T_{cons} and T_{dec}) were used as inputs to design the trapezoidal motion profiles. Selection of the T_{dec} time as an integer multiple of the fundamental period of the manipulator proved that the residual vibrations were suppressed significantly (Karagülle et al., 2017; Malgaca et al., 2016; Yavuz et al., 2016). The motion time parameters of trapezoidal velocity profile were defined by the vector $\mathbf{qt}_m$ = [T_{acc}, T_{cons}, T_{dec}, T_m].

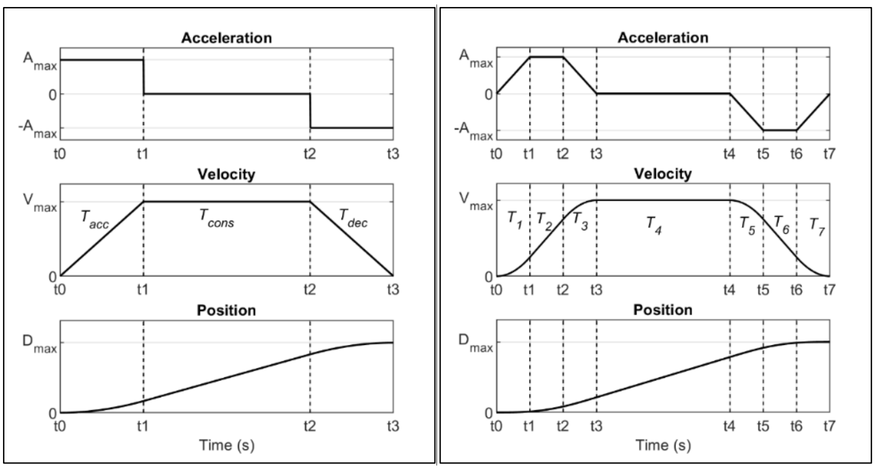

(a) (b)

Figure 2.3 (a) Trapezoidal velocity motion profile (b) 3rd order S-curve velocity motion profile

V_{max} value of trapezoidal motion profile design can be calculated as shown in Eq. (2.16).

$$V_{max} = \frac{D_{max}}{0.5T_{acc} + 0.5T_{dec} + T_{cons}} \tag{2.16}$$

For $t \in [t_0, t_1]$,

$$a(t) = A_{max} \tag{2.17}$$

$$v(t) = \frac{V_{max}}{T_{acc}} t \tag{2.18}$$

$$d(t) = \frac{V_{max}}{2T_{acc}} t^2 \tag{2.19}$$

For $t \in [t_1, t_2]$,

$$a(t) = 0 \tag{2.20}$$

$$v(t) = V_{max} \tag{2.21}$$

$$d(t) = V_{max}(t - t_1) + \frac{V_{max}}{2} T_{acc} \tag{2.22}$$

For $t \in [t_2, t_3]$,

$$a(t) = -A_{max} \tag{2.23}$$

$$v(t) = V_{max} - \frac{V_{max}}{T_{dec}}(t - t_2) \tag{2.24}$$

$$d(t) = V_{max}(t - t_2) - \frac{V_{max}}{2T_{dec}}(t - t_2)^2 + V_{max}T_{cons} + \frac{V_{max}}{2}T_{acc} \tag{2.25}$$

The S-curve motion profile and all-time parameters are shown in Figure 2.3 (b). The acceleration and deceleration times of velocity motion profiles were selected equal. In order to design the motion profile, all time parameters ($T_{i,}$ i=1,2,3…,7) and travel distance (D_{max}) were given as inputs. By using these inputs, maximum velocity and acceleration values were calculated. The 3rd order S-curve motion profile has seven-time segments, and each time segment takes a time interval of $T_{i,}$ i=1,2,3…,7. Total motion time (T_m) can be calculated as the sum of these seven-time segments. The motion profiles were designed symmetrical. For these boundary condition, T_1=T_3=T_5=T_7 and T_2=T_6. Then T_m=4T_1+2T_2+T_4. At an arbitrary time t, the equations of acceleration, velocity and angular displacement of S-curve motion profile at a specific time interval are given from Eq. (2.26) to Eq. (2.46). The final values of velocity and angular position at a specific phase were also given to calculate the A_{max}. V_i and D_i values represent the velocity and displacement values at an arbitrary time t_i, i=1,2,3…7. The 3rd order motion profile time parameters were defined by the vector **qs**$_m$ = [T_1, T_2, T_3, T_m].

For $t \in [t_0, t_1]$,

$$a(t) = A_{max}\frac{t}{T_1} \tag{2.26}$$

$$v(t) = A_{max}\frac{t^2}{2T_1} \rightarrow V_1 = A_{max}\frac{T_1}{2} \tag{2.27}$$

$$d(t) = A_{max}\frac{t^3}{6T_1} \rightarrow D_1 = A_{max}\frac{T_1^2}{6} \qquad (2.28)$$

For $t \in [t_1, t_2]$,

$$a(t) = A_{max} \qquad (2.29)$$

$$v(t) = V_1 + A_{max}(t - t_1) \rightarrow V_2 = V_1 + A_{max}T_2 \qquad (2.30)$$

$$d(t) = D_1 + V_1(t - t_1) + A_{max}\frac{(t - t_1)^2}{2} \rightarrow D_2 = D_1 + V_1T_2 + A_{max}\frac{T_2^2}{2} \qquad (2.31)$$

For $t \in [t_2, t_3]$,

$$a(t) = A_{max} - A_{max}\frac{(t - t_2)}{T_3} \qquad (2.32)$$

$$v(t) = V_2 + A_{max}(t - t_2) - A_{max}\frac{(t - t_2)^2}{2T_3} \rightarrow V_{max} = V_3 = V_2 + A_{max}\frac{T_3}{2} \qquad (2.33)$$

$$\begin{aligned} d(t) &= D_2 + V_2(t - t_2) + A_{max}\frac{(t - t_2)^2}{2} - A_{max}\frac{(t - t_2)^3}{6T_3} \\ D_3 &= D_2 + V_2T_3 + A_{max}\frac{T_3^{\,2}}{3} \end{aligned} \qquad (2.34)$$

For $t \in [t_3, t_4]$,

$$a(t) = 0 \qquad (2.35)$$

$$v(t) = V_{max} \rightarrow V_4 = V_{max} \qquad (2.36)$$

$$d(t) = D_3 + V_{max}(t - t_3),\ D_4 = D_3 + V_{max}T_4 \qquad (2.37)$$

For $t \in [t_4, t_5]$,

$$a(t) = -A_{max}\frac{(t - t_4)}{T_5} \qquad (2.38)$$

$$v(t) = V_{max} - A_{max}\frac{\left(t-t_4\right)^2}{2T_5} \rightarrow V_5 = V_{max} - A_{max}\frac{T_5}{2} \tag{2.39}$$

$$\begin{gathered} d(t) = D_4 + V_{max}\left(t-t_4\right) - A_{max}\frac{\left(t-t_4\right)^3}{6T_5} \\ D_5 = D_4 + V_{max}T_5 - A_{max}\frac{T_5^{\ 2}}{6} \end{gathered} \tag{2.40}$$

For $t \in \left[t_5, t_6\right]$,

$$a(t) = -A_{max} \tag{2.41}$$

$$v(t) = V_5 - A_{max}(t-t_5) \rightarrow V_6 = V_5 - A_{max}T_6 \tag{2.42}$$

$$\begin{gathered} d(t) = D_5 + V_5(t-t_5) - A_{max}\frac{(t-t_5)^2}{2} \\ D_6 = D_5 + V_5T_6 - A_{max}\frac{T_6^2}{2} \end{gathered} \tag{2.43}$$

For $t \in \left[t_6, t_7\right]$,

$$a(t) = A_{max}\frac{(t-t_6)}{T_7} - A_{max} \tag{2.44}$$

$$v(t) = V_6 - A_{max}(t-t_6) + A_{max}\frac{(t-t_6)^2}{2T_7} \rightarrow V_7 = 0 = V_6 - A_{max}\frac{T_7}{2} \tag{2.45}$$

$$\begin{gathered} d(t) = D_6 + V_6(t-t_6) - A_{max}\frac{(t-t_6)^2}{2} + A_{max}\frac{(t-t_6)^3}{6T_7} \\ D_7 = D_6 + V_6T_7 - A_{max}\frac{T_7^{\ 2}}{3} \end{gathered} \tag{2.46}$$

$$A_{max} = \frac{D_{max}}{(T_1+T_2)(2T_1+T_2+T_4)} \tag{2.47}$$

After obtaining all the equations by using inputs (D_{max} and T_i i=1,2,3…7), it was observed that all the equations are dependent A_{max} value. A_{max} value can be found as shown in Eq. (2.47). After obtaining A_{max}, all values of acceleration, velocity and position can be calculated for all time steps of the desired motion time.

2.4 The Effect of S-Curve Motion Profile Time Parameters on Transient and Residual Vibrations

In the study of the Byeogjin Kim et al. (B. Kim et al., 2017) it was shown that the selection of the 3rd order polynomial S-curve motion profile time parameters as integer multiples of the natural period of an undamped two degree of freedom system causes zero residual vibrations. Simulations using the motion cases in Table 2.3 were performed, in order to observe the effects of the S-curve motion time parameters on the transient and residual vibrations of the designed flexible manipulator which has properties given in Table 2.2. The approach presented in the study of Byeogjin Kim et al. (B. Kim et al., 2017) was also taken into consideration during the design of the motion cases in order to observe whether it also works on a multi-DOF dumped system or not.

Table 2.3 Motion case-1 for 3rd order S-curve velocity motion profiles

Case-1/ S-curve	**$[D_0, D_{max}]$**	**T_m-T_{res}**	**Schematic**	**t1h (Newmark)**	**t1h (ANSYS)**
[3.25t1h, 3.5t1h, 3.25t1h, T_m] [3t1h, 4t1h, 3t1h, T_m] [4t1h, 3t1h, 4t1h, T_m] [4t1h, 2t1h, 4t1h, T_m]	[0,90]	1.32s-2s	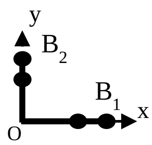	1/8.3331/2 ≈0.06s	1/8.3329/2 ≈0.06s

The acceleration and deceleration times of motion profiles were selected equal. The 3rd order motion profile time parameters were defined by the vector $\mathbf{qs}_m = [T_1, T_2, T_3, T_m]$ as mentioned before. The simulations were performed for the same total motion angle D_{max} and the same time motion which is T_m. T_m is selected as 22t1h for motion cases. The total analysis time was defined as T_{res}=2s in order to observe the residual vibrations for all performed analyses. t1h is equal to half of the fundamental natural period of the manipulator.

The vibration responses of both Ansys and Newmark solution are given for comparison. It is seen from Figure 2.4 (a) and (b) that the Newmark solution very well fit the Ansys solution. The response differences between Newmark and ANSYS solutions are very small, and these differences are acceptable. After this validation, only Newmark solution results will be presented. It can be seen in Figure 2.5 the selection of the time parameter as integer multiple of the natural period gives better results.

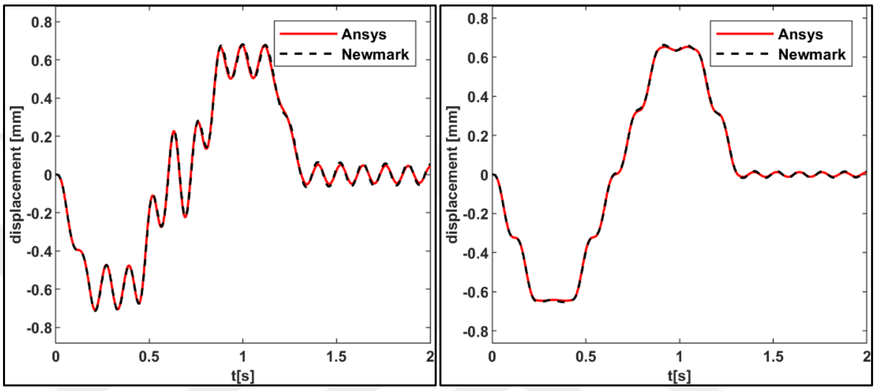

(a) (b)

Figure 2.4 Vibration response comparison between Ansys and Newmark solution for Case 1 qsm=[3t1h, 4t1h, 3t1h, Tm] for (a), qsm=[4t1h, 3t1h, 4t1h, Tm] for (b)

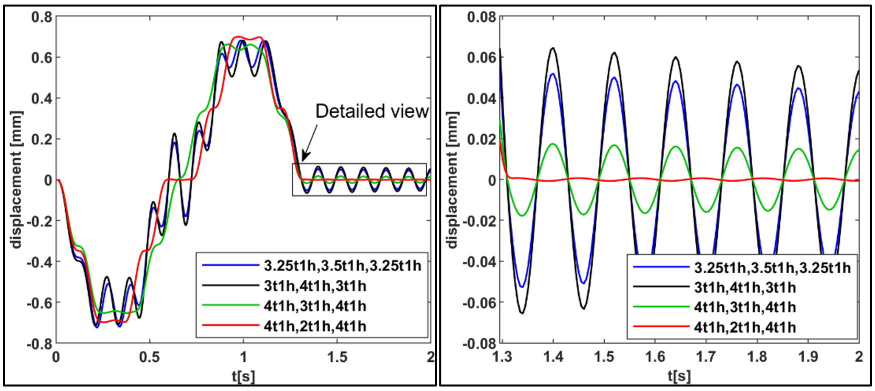

(a) (b)

Figure 2.5 (a) Transient and residual vibrations responses for all motions of Case-1 (b) detailed view of residual vibrations

The maximum transient and residual amplitude values and maximum velocity and acceleration values of the motion profiles that were reached are given in Table 2.4.

Although the $\mathbf{qs}_m$=[4t1h, 2t1h ,4t1h, T_m] reaches th"e maximum acceleration, it has the minimum residual vibration amplitudes. The reason behind this is that the motion profile parameters were selected as integer multiples of the first natural period.

Table 2.4 The obtained results of Case-1 motion profiles

Case-1/ S-curve	**V_{max} (rad/s)**	**A_{max} (rad/s^2)**	**Max. Ampl. (mm)**	**Max. Res Ampl. (μm)**
[3.25t1h,3.5t1h,3.25t1h,T_m]	2.1817	5.3868	0.7233	52.7136
[3t1h,4t1h,3t1h,T_m]	2.1817	5.1944	0.7148	65.6206
[4t1h,3t1h,4t1h,T_m]	2.38	5.6667	0.662	17.7858
[4t1h,2t1h,4t1h,T_m]	2.1817	6.0602	0.6989	0.7295

2.5 The Comparison of S-Curve and Trapezoidal Motion Profile Results

In this part the comparison of the residual and transient vibration results between the proposed 3rd order S-curve velocity motion profiles and proposed trapezoidal velocity motion profiles (Karagülle et al., 2017; Malgaca et al., 2016; Yavuz et al., 2016) is shown. When the T_{dec} time parameter was defined as an integer multiple of the natural period, the residual vibrations were suppressed significantly (Ankarali & Diken, 1997; Karagülle et al., 2017; Malgaca et al., 2016; Yavuz et al., 2016). In order to make an appropriate comparison between the results under two different types of motion profiles, acceleration and deceleration times of both motion profiles were selected equal. Symmetrical motion profiles were used. The definitions of the motion vectors were given as $\mathbf{qt}_m$ = [T_{acc}, T_{cons}, T_{dec}, T_m] and $\mathbf{qs}_m$ = [T_1, T_2, T_3, T_m] in the previous section. The simulations were performed for the same rotation angle (D_{max}) and different motion time (T_m). If one motion time parameter in the motion vector representation was not half or a multiple integer of the natural period, then that motion time parameters was written as (*) in motion vector. The defined motion cases for transient analyses were given in Table 2.5. t1h is the time which is the half of the fundamental natural period of the manipulator.

Table 2.5. Motion Cases for trapezoidal and S-curve motion profiles

Cases		**[D_0, D_{max}]**	**T_m-T_{res}**
Case2			
S-curve	**Trapezoidal**		
[2t1h, 0 ,2t1h, T_m] [2t1h, 2t1h, 2t1h, T_m] [2t1h, 4t1h, 2t1h, T_m] [2t1h, 6t1h, 2t1h, T_m] [4t1h, 0, 4t1h, T_m] [4t1h, 2t1h, 4t1h, T_m]	[4t1h, 12t1h, 4t1h, T_m] [6t1h, 8t1h, 6t1h, T_m] [8t1h, 4t1h,8t1h, T_m] [10t1h, 0, 10t1h, T_m] [8t1h, 4t1h, 8t1h, T_m] [10t1h, 0, 10t1h, T_m]	[0,90]	1.2s-2s
Case3		**[D_0, D_{max}]**	**T_m-T_{res}**
S-curve	**Trapezoidal**		
[2t1h, 0, 2t1h, Tm] [2t1h, 2t1h, 2t1h, Tm] [2t1h, 4t1h, 2t1h, Tm] [4t1h, 0, 4t1h, Tm]	[4t1h, *, 4t1h, Tm] [6t1h, *, 6t1h, Tm] [8t1h, *, 8t1h, Tm] [8t1h, *, 8t1h, Tm]	[0,90]	1s-2s
Case4		**[D_0, D_{max}]**	**T_m-T_{res}**
S-curve	**Trapezoidal**		
[2t1h, 0, 2t1h, Tm]	[4t1h, 0, 4t1h, Tm]	[0,90]	0.48s-2s

The motion profiles of Case2 have 1.2s as motion time and all the-time parameters were selected as integer multiple of first natural period of flexible manipulator for both motion profiles. The motion profiles in Case3 have 1s motion time and the time parameters were selected as integer multiple of first natural period of the manipulator besides T_4 and T_{cons}. In Case4 the S-curve motion profile was designed in order to perform the same job of Case2 and Case3 in the shortest time. The time parameters T_1, T_2 and T_4 were selected as one natural period of the flexible manipulator, zero and zero respectively in Case4.

The vibration response results under the given motion profiles for Case2 qsm=[2t1h, 6t1h, 2t1h, Tm] and qtm=[10t1h, 0, 10t1h, Tm] are given in (a). The maximum vibration amplitudes for the transient and residual regions were also shown in Figure 2.6 (a) and (b) respectively. Similar the vibration responses for given motion profiles for Case3 qsm=[2t1h, 2t1h, 2t1h, Tm] and qtm=[6t1h, *, 6t1h, Tm] were also shown in Figure 2.7 (a). The detailed view in Figure 2.7 (a) and maximum vibration amplitudes for residual vibrations were shown in Figure 2.7 (b). The maximum vibration amplitudes and the amount of the reductions in percentage for both transient and residual regions were given in Table 2.6 and Table 2.7. The reached maximum acceleration and velocity values were also included in both Table 2.6 and Table 2.7 for Case2, Case3 and Case4.

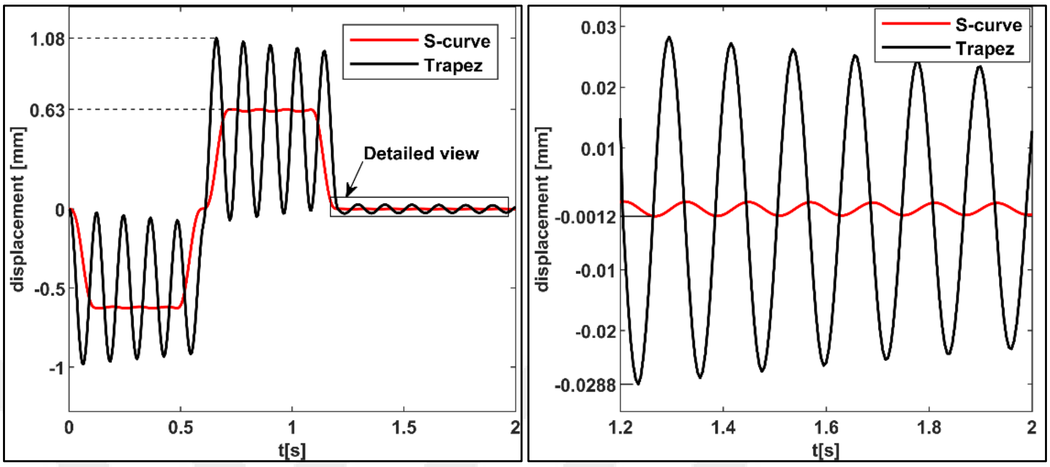

(a) (b)

Figure 2.6 Vibration results (a) for Case2 qs_m=[2t1h, 6t1h, 2t1h, T_m], qt_m=[10t1h, 0, 10t1h, T_m] (b) Detailed view of residual region of (a)

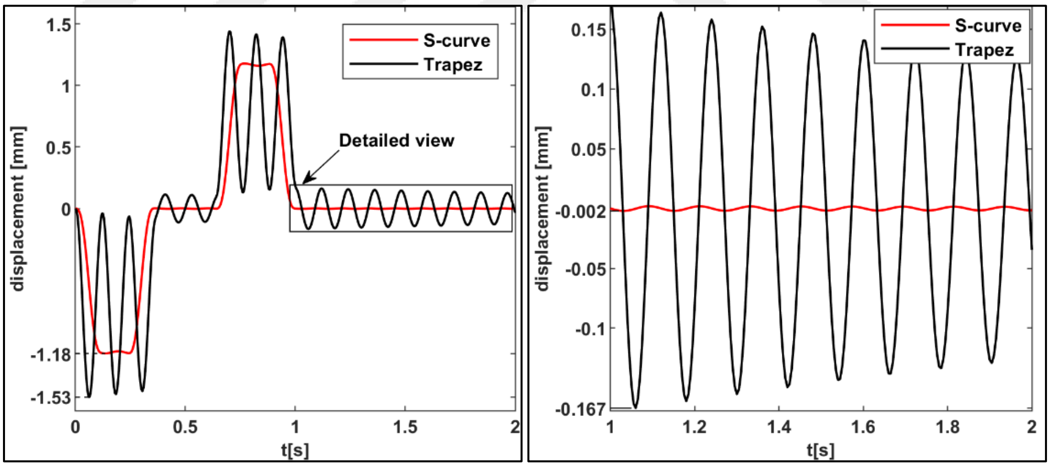

(a) (b)

Figure 2.7 Vibration results (a) for Case3 qs_m=[2t1h, 2t1h, 2t1h, T_m], qt_m=[6t1h, *, 6t1h, T_m] (b) Detailed view of residual region of (a)

Table 2.6 The Results of Case2

Case2											
S-curve	**Trapezoidal**	**V_{max}** (rad/s) **qs_m** and **qt_m**	**A_{max}** (rad/s^2)		**%Max Amp. Decay**	**%Max Res. Amp. Decay**	**Max. Amp.** (mm)		**Max. Res. Amp.** (μm)	
			qs_m	**qt_m**			**qs_m**	**qt_m**	**qs_m**	**qt_m**
[2t1h, 0, 2t1h, T_m]	[4t1h, 12t1h, 4t1h, T_m]	1.64	13.6	6.82	1.164	96.15	1.57	1.59	1.08	28.1
[2t1h, 2t1h, 2t1h, T_m]	[6t1h, 8t1h, 6t1h, T_m]	1.87	7.79	5.19	27.14	97.09	0.89	1.23	0.83	28.4
[2t1h, 4t1h, 2t1h, T_m]	[8t1h, 4t1h, 8t1h, T_m]	2.18	6.06	4.55	36.49	96.85	0.699	1.10	0.90	28.7
[2t1h, 6t1h, 2t1h, T_m]	[10t1h, 0, 10t1h, T_m]	2.62	5.45	4.36	41.61	95.75	0.63	1.08	1.23	28.8
[4t1h, 0, 4t1h, T_m]	[8t1h, 4t1h, 8t1h, T_m]	2.18	9.09	4.55	5.003	96.42	1.05	1.10	1.03	28.7
[4t1h, 2t1h, 4t1h, T_m]	[10t1h, 0, 10t1h, T_m]	2.62	7.27	4.36	22.28	95.23	0.84	1.08	1.37	28.8

Table 2.7 The results of Case3 and Case4

Case3										
S-curve	**Trapezoidal**	**V_{max}** (rad/s) **qs_m** and **qt_m**	**A_{max}** (rad/s^2)		**%Max Amp. Decay**	**%Max Res. Amp. Decay**	**Max. Amp.** (mm)		**Max. Res. Amp.** (μm)	
			qs_m	**qt_m**			**qs_m**	**qt_m**	**qs_m**	**qt_m**
[2t1h, 0, 2t1h, T_m]	[4t1h, *, 4t1h, T_m]	2.067	17.2	8.61	-2.32	98.1	1.98	1.93	2.61	137.3
[2t1h, 2t1h, 2t1h, T_m]	[6t1h, *, 6t1h, T_m]	2.454	10.2	6.82	23.13	98.81	1.18	1.53	1.99	166.8
[2t1h, 4t1h, 2t1h, T_m]	[8t1h, *, 8t1h, T_m]	3.021	8.39	6.29	31.62	98.89	0.97	1.41	2.35	211.5
[4t1h, 0, 4t1h, T_m]	[8t1h, *, 8t1h, T_m]	3.021	12.6	6.29	-2.37	98.78	1.45	1.41	2.59	211.5
Case4										
[2t1h, 0, 2t1h, T_m]	[4t1h, 0, 4t1h, T_m]	6.545	54.5	27.3	1.728	2.56	6.37	6.49	91.8	94.23

In order to make a proper comparison between the S-curve and trapezoidal motion profiles results, the maximum velocities that were reached for both motion profiles were selected equal by defining the same acceleration and deceleration times for both motion profiles. Although the S-curve motion profiles reached higher acceleration values, the vibration amplitudes seem to be better than the trapezoidal ones in terms of both transient and residual vibrations for all motion cases in Case2 according to the results given in Table 2.6. The existence and value of T_2 caused less maximum transient vibration amplitudes even if the acceleration times were selected equal such as between the results of **qs_m**=[2t1h, 4t1h, 2t1h, Tm] and **qs_m**=[4t1h, 0, 4t1h, Tm] for both Case2 and Case3 and **qs_m**=[2t1h, 6t1h, 2t1h, Tm] and **qs_m**=[4t1h, 2t1h, 4t1h, Tm] for Case2. When the S-curve motion profiles which have the same acceleration times were investigated, the use of only T_1 in the acceleration time without using T_2 causes high acceleration values and high transient vibration amplitudes. For this reason, T_1 should be selected as short as possible and T2 can be selected as any integer multiple of the first natural period of the flexible manipulator depending on Tm. All the time parameters of the motion profiles in Case2 were selected as integer multiples of the fundamental natural period of the manipulator for both the S-curve and the trapezoidal motion profiles. If all the time parameters of both motion profiles were selected as integer multiples of the natural period of the manipulator or zero, the maximum residual vibration amplitudes did not vary from one motion profile to another, as can be seen from Table 2.6.

The effects of T_{cons} and T_4 not being chosen as the integer multiples of the natural period on the vibration results are shown in Table 2.7 for the motion profiles of Case3. While it was observed that T_4 not being an integer multiple of the natural period has no effect on the vibration results, it was understood that Tcons not being an integer multiple of the natural period has an important effect on the residual vibration results. The trapezoidal motion profile gave almost the same result with a few differences for the minimum motion time in Case4. The S-curve motion profiles maximum residual vibration amplitudes was related with reaching both maximum velocity and acceleration values as shown in Table 2.6 and Table 2.7.

In motion Case3 the change of the amplitudes in the S-curve motion profile results from one motion to another one was less than the trapezoidal motion profile results in terms of maximum residual amplitude. It was observed that the amount of T_{cons} was effective on these results. In order to make an investigation on the effect of the T_4 and T_{cons} amount on the residual vibration amplitudes, a new motion Case study was defined and showed in Table 2.8. The effect of T_2 on both the residual and transient vibrations was explained as mentioned before. In the design of Case5 motion profiles, given in Table 2.8, the acceleration and deceleration times were selected equal for both motion profiles, and the time parameter T_2 of S-curve motion profiles selected as 4t1h seconds. T_4 and T_{cons} time parameters were selected from 0 to 4t1h by changing the motion time T_m.

Table 2.8 Motion case for the investigation on the effect of the T_4 and T_{cons} on the residual vibrations

Case5		**T_m-T_{res}**	**[D_0, D_{max}]**
S-curve	**Trapezoidal**		
[2t1h, 4t1h, 2t1h, T_m]	[8t1h, 0, 8t1h, T_m]	0.96s-2s	[0,90]
	[8t1h, *,8t1h, T_m]	0.98s-2s	
	[8t1h, *,8t1h, T_m]	1s-2s	
	[8t1h, t1h, 8t1h, T_m]	1.02s-2s	
	[8t1h, *, 8t1h, T_m]	1.04s-2s	
	[8t1h, *, 8t1h, T_m]	1.06s-2s	
	[8t1h, 2t1h, 8t1h, T_m]	1.08s-2s	
	[8t1h, *, 8t1h, T_m]	1.1s-2s	
	[8t1h, *, 8t1h, T_m]	1.12s-2s	
	[8t1h, 3t1h, 8t1h, T_m]	1.14s-2s	
	[8t1h, *, 8t1h, T_m]	1.16s-2s	
	[8t1h, *, 8t1h, T_m]	1.18s-2s	
	[8t1h, 4t1h, 8t1h, T_m]	1.2s-2s	

The results of Case5 motion profiles are shown in Table 2.9. If T1 and T2 were selected as integer multiples of the natural period of the flexible manipulator, the selection of T_4 either as any multiple of the natural period of the manipulator or as zero does not affect the maximum residual vibration amplitudes according to the data given Table 2.9. The maximum residual vibration amplitudes of S-curve motion profiles results decreased linearly when T_4 increased, which causes the decrement of both the maximum velocity and acceleration values that were reached. The increment of T_{cons} does not cause a linear decrement on the maximum residual vibration amplitudes of the trapezoidal motion profile results. It can be seen in Table 2.9 that the minimum residual vibration amplitudes for trapezoidal motion profiles occurred when the T_{cons} were selected as an integer multiple of the first natural period of the manipulator. The effects of T_4 and T_{cons} on the maximum residual vibration amplitudes were shown in Figure 2.8 (a) and (b) for both trapezoidal and S-curve motion profiles respectively.

Table 2.9 The result of Case5

Case5								
S-curve	**Trapezoidal**	**Tm-Tres (sec.)**	**%Max Amp. Decay**	**%Max Res. Amp. Decay**	**Max. Amp.** (mm)		**Max. Res. Amp.** (μm)	
					qs_m	**qt_m**	**qs_m**	**qt_m**
[2t1h, 4t1h, 2t1h, T_m]	[8t1h, 0, 8t1h, T_m]	0.96-2	36.62	88.66	1.053	1.661	3.548	31.293
[2t1h, 4t1h, 2t1h, T_m]	[8t1h, *,8t1h, T_m]	0.98-2	31.41	97.45	1.008	1.47	2.956	115.82
[2t1h, 4t1h, 2t1h, T_m]	[8t1h, *,8t1h, T_m]	1-2	31.62	98.89	0.967	1.414	2.347	211.54
[2t1h, 4t1h, 2t1h, T_m]	[8t1h, t1h, 8t1h, T_m]	1.02-2	31.65	99.2	0.93	1.361	1.99	247.88
[2t1h, 4t1h, 2t1h, T_m]	[8t1h, *, 8t1h, T_m]	1.04-2	33.48	99.13	0.899	1.352	1.905	218.2
[2t1h, 4t1h, 2t1h, T_m]	[8t1h, *, 8t1h, T_m]	1.06-2	37.35	98.63	0.87	1.388	1.852	134.85
[2t1h, 4t1h, 2t1h, T_m]	[8t1h, 2t1h, 8t1h, T_m]	1.08-2	36.57	94.28	0.841	1.325	1.704	29.794
[2t1h, 4t1h, 2t1h, T_m]	[8t1h, *, 8t1h, T_m]	1.1-2	31.52	98.24	0.812	1.186	1.547	87.998
[2t1h, 4t1h, 2t1h, T_m]	[8t1h, *, 8t1h, T_m]	1.12-2	31.67	99.06	0.785	1.148	1.545	164.5
[2t1h, 4t1h, 2t1h, T_m]	[8t1h, 3t1h, 8t1h, T_m]	1.14-2	31.68	99.2	0.761	1.114	1.564	195.94
[2t1h, 4t1h, 2t1h, T_m]	[8t1h, *, 8t1h, T_m]	1.16-2	33.13	99.18	0.74	1.106	1.435	175.07
[2t1h, 4t1h, 2t1h, T_m]	[8t1h, *, 8t1h, T_m]	1.18-2	37.05	98.95	0.72	1.143	1.171	111.76
[2t1h, 4t1h, 2t1h, T_m]	[8t1h, 4t1h, 8t1h, T_m]	1.2-2	36.49	96.85	0.7	1.102	0.903	28.656

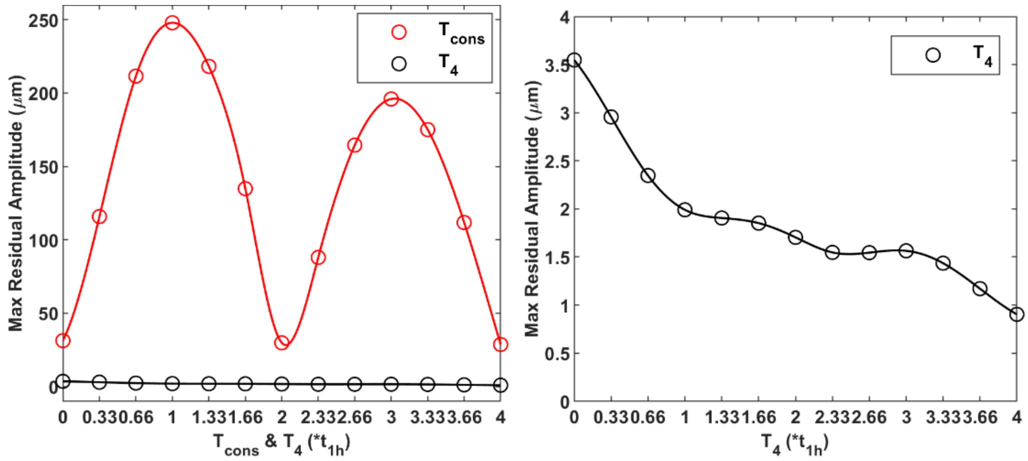

(a) (b)

Figure 2.8 (a) Effect of T_4 and T_{cons} (b) The effect of T_4 detailed

2.6. Conclusions

In this part of the study, the effects of both the S-curve and the trapezoidal motion time parameters on the transient and residual vibrations of a flexible manipulator were investigated. When the S-curve motion profile time parameters were defined as an integer multiple of the fundamental natural period of the flexible manipulator, the residual vibrations were reduced effectively. The comparison between the S-curve motion profiles and the trapezoidal motion profile results were also investigated for different motion cases. It was observed that the residual and transient vibrations amplitudes of the manipulator under the S-curve motion profiles were less than the trapezoidal motion profiles, even if they reached the same maximum velocity. The S-curve motion profiles reached higher acceleration values than trapezoidal motion profiles. It was found that the presence of T_2 which is a S-curve motion time parameter caused the smallest maximum transient vibration amplitudes when the results of S-curve motion profiles which have the same acceleration time were compared. It can be concluded that for the S-curve motion profiles the selection of T_4 as any multiple of the first natural period of the flexible manipulator or zero did not affect the residual vibration amplitudes. However, for the trapezoidal motion profiles the selection of T_{cons} as an integer multiple of the first natural period of the flexible manipulator is important to reduce the residual vibration amplitudes. In order to obtain minimum residual vibration amplitudes under the trapezoidal velocity motion profile, all the time parameters should be selected as integer multiples of the fundamental natural period of the flexible manipulator. In the case of the S-curve motion profile, all time parameters besides T_4 should be selected as integer multiples of the first natural period of the manipulator according to the obtained results. In terms of residual vibration amplitudes, it was observed that the motion profiles of Case2 do not have a significant advantage compared to each other among the same type of motion profile. This conclusion is valid for both 3rd order polynomial S-curve and trapezoidal motion profiles. However, the acceleration time should be selected long, if possible, for both S-curve and trapezoidal motion profiles in order to reduce transient vibration amplitudes. In order to obtain the minimum transient vibration amplitudes for S-curve motion profiles, T_1 should be at least equal to 2t1h and T_2 should be selected as long as possible depending on T_m. The T_{acc} and T_{dec} times of the trapezoidal motion profiles should be selected as long as possible and T_{cons} should be selected as short as possible in order to obtain less transient vibration amplitudes.

CHAPTER THREE
INVESTIGATION OF PERFORMANCE AND SENSITIVITY OF S-CURVE MOTION PROFILES ON REDUCTION OF FLEXIBLE MANIPULATOR VIBRATIONS

3.1 Methodology

In this chapter, passive vibration control was achieved by designing three different velocity motion profiles with seven segments. The effect of these motion profiles on the end point transient and residual vibrations of a flexible manipulator were studied experimentally (Akdağ & Şen, 2023) and by performing finite element simulations in ANSYS. These motion profiles were 3^{rd} order polynomial S-curves and two different trigonometric (harmonic and pure sinusoidal) S-curve motion profiles. Symmetrical velocity motion profiles which have equal acceleration and deceleration times were used, and time parameters of these motion profiles were defined either half-integer multiples or integer multiples of flexible manipulator's fundamental natural period. The results of the experiments were compared with the transient analysis results obtained from ANSYS. The effects of time parameters of all motion profiles on endpoint vibrations were shown by comparing them in terms of amplitudes. Errors in the natural frequency measurements of the flexible manipulator change the time parameters of the motion profiles, and this change adversely affects the endpoint passive vibration control. The sensitivity of vibration results to 4% natural frequency measurement error was shown for three motion profiles.

3.2 Design of S-Curve Motion Profiles and Definition of Motion Vectors

In this part the design of all velocity motion profiles which were used to actuate the flexible manipulator will be explained. These motion profiles were named as 3^{rd} order polynomial S-curve motion profile, harmonic sinusoidal motion profile and pure sinusoidal motion profile. All of the motion profiles have seven time region ($T_{1,2,3..7}$). The time parameters ($T_{1,2,3..7}$) and rotational motion distance (θ or D_{max}) were given as inputs to design the motion profiles. The velocity motion profiles were designed symmetrically which means the acceleration and deceleration times are equal. All three motion profiles and their time parameters are shown in Figure 3.1.

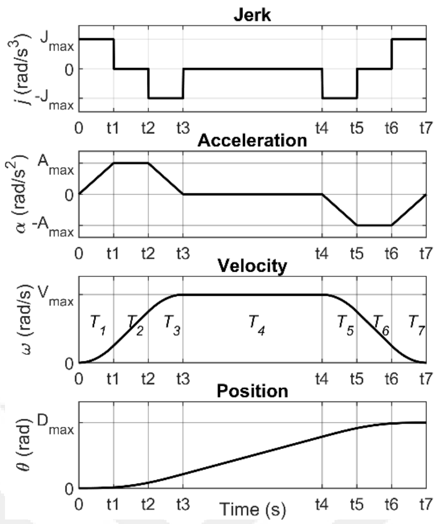

(a)

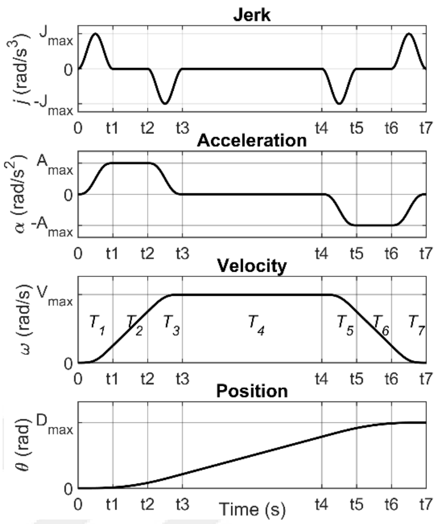

(b)

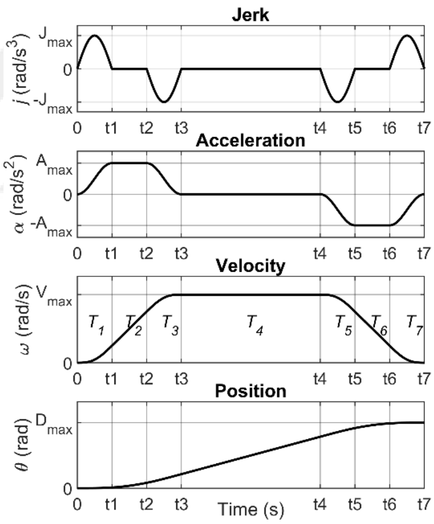

(c)

Figure 3.1 (a) Polynomial S-curve Motion Profile, (b) Harmonic Sinusoidal Motion Profile (c) Pure Sinusoidal Motion Profile

In the symmetrical condition T_1=T_3=T_5=T_7 and T_2=T_6.Therefore the total motion time is going to be T_m=4T_1+2T_2+T_4 and the motion profile can be designed using only T_1 and T_2. All motion profiles were derived from the Jerk equations as in most of the studies, by giving the maximum Jerk value as an input then calculates the time parameters (B. Kim et al., 2017; HZ Li et al., 2006; Huaizhong Li et al., 2009; Nguyen et al., 2008). The Jerk equations of the 3rd order polynomial S-curve motion profile (J_s), harmonic sinusoidal motion profile (J_{hsin}) and pure sinusoidal motion profile (J_{psin}) were given in Eq. (3.1), Eq. (3.2) and Eq. (3.3) respectively.

$$J_s = \dddot{\theta}_s = \begin{Bmatrix} J_{s\_max} & \text{for } 0 \le t \le t_1 \\ 0 & \text{for } t_1 < t \le t_2 \\ -J_{s\_max} & \text{for } t_2 < t \le t_3 \\ 0 & \text{for } t_3 < t \le t_4 \\ -J_{s\_max} & \text{for } t_4 < t \le t_5 \\ 0 & \text{for } t_5 < t \le t_6 \\ J_{s\_max} & \text{for } t_6 < t \le t_7 \end{Bmatrix} \tag{3.1}$$

$$J_{h\sin} = \dddot{\theta}_{h\sin} = \begin{Bmatrix} \frac{J_{h\sin\_max}}{2}\left[1-\sin\left(\frac{2\pi}{T_1}t+\frac{\pi}{2}\right)\right] & \text{for } 0 \le t \le t_1 \\ 0 & \text{for } t_1 < t \le t_2 \\ -\frac{J_{h\sin\_max}}{2}\left[1-\sin\left(\frac{2\pi}{T_3}(t-t_2)+\frac{\pi}{2}\right)\right] & \text{for } t_2 < t \le t_3 \\ 0 & \text{for } t_3 < t \le t_4 \\ -\frac{J_{h\sin\_max}}{2}\left[1-\sin\left(\frac{2\pi}{T_5}(t-t_4)+\frac{\pi}{2}\right)\right] & \text{for } t_4 < t \le t_5 \\ 0 & \text{for } t_5 < t \le t_6 \\ \frac{J_{h\sin\_max}}{2}\left[1-\sin\left(\frac{2\pi}{T_7}(t-t_6)+\frac{\pi}{2}\right)\right] & \text{for } t_6 < t \le t_7 \end{Bmatrix} \tag{3.2}$$

The use of acceleration equations was preferred. According to the defined inputs ($T_{1,2,3\ldots7}$ and D_{max}) the maximum values of jerk equations J_{s_max}, J_{hsin_max} and J_{psin_max} cannot be calculated directly, and acceleration and velocity equations cannot be derived either. However, by using the given inputs ($T_{1,2,3\ldots7}$ and D_{max}) V_{max} (reached maximum velocity) can be calculated by using Eq. (3.4), since the area under the velocity graph gives the distance. A_{max} (reached maximum acceleration) value can also be calculated by using given Eq. (3.5) using the same approach. Eq. (3.4) and Eq. (3.5) are only valid for symmetrical motion profiles.

$$J_{psin} = \dddot{\theta}_{psin} = \left\{ \begin{array}{cl} J_{psin\_max}\left[\sin\left(\dfrac{\pi}{T_1}t\right)\right] & \text{for } \ 0 \le t \le t_1 \\ 0 & \text{for } t_1 < t \le t_2 \\ -J_{psin\_max}\left[\sin\left(\dfrac{\pi}{T_3}(t-t_2)\right)\right] & \text{for } t_2 < t \le t_3 \\ 0 & \text{for } t_3 < t \le t_4 \\ -J_{psin\_max}\left[\sin\left(\dfrac{\pi}{T_5}(t-t_4)\right)\right] & \text{for } t_4 < t \le t_5 \\ 0 & \text{for } t_5 < t \le t_6 \\ J_{psin\_max}\left[\sin\left(\dfrac{\pi}{T_7}(t-t_6)\right)\right] & \text{for } t_6 < t \le t_7 \end{array} \right\} \tag{3.3}$$

$$V_{max} = \frac{D_{max}}{2T_1 + T_2 + T_4} \tag{3.4}$$

$$A_{max} = \frac{V_{max}}{T_1 + T_2} \tag{3.5}$$

When the same inputs ($T_{1,2,3\ldots7}$ and D_{max}) are used to design all the motion profiles both A_{max} and V_{max} values are going to be equal for all motion profile types. Therefore, acceleration equations were written in terms of A_{max}. The relationship between the A_{max} and maximum Jerk values are given in Eq. (3.6).

$$J_{s\_max} = \frac{A_{max}}{T_1},\ J_{hsin\_max} = \frac{2A_{max}}{T_1},\ J_{psin\_max} = \frac{\pi A_{max}}{2T_1} \tag{3.6}$$

The acceleration equations were also derived by integrating the jerk equations. The acceleration equations of the 3rd order polynomial S-curve motion profile, harmonic sinusoidal motion profile and pure sinusoidal motion profile are given in Eq. (3.7), Eq. (3.8) and Eq. (3.9) respectively. The velocity equations were also derived by integrating the acceleration equations. The velocity equations of the 3rd order polynomial S-curve motion profile, harmonic sinusoidal motion profile and pure sinusoidal motion profile are given in Eq. (3.10), Eq. (3.11) and Eq. (3.12) respectively.

$$\ddot{\theta}_s = \begin{cases} A_{max}\dfrac{t}{T_1} & \text{for } 0 \le t \le t_1 \\ A_{max} & \text{for } t_1 < t \le t_2 \\ A_{max} - A_{max}\dfrac{(t-t_2)}{T_3} & \text{for } t_2 < t \le t_3 \\ 0 & \text{for } t_3 < t \le t_4 \\ -A_{max}\dfrac{\left(t-t_4\right)}{T_5} & \text{for } t_4 < t \le t_5 \\ -A_{max} & \text{for } t_5 < t \le t_6 \\ A_{max}\dfrac{(t-t_6)}{T_7} - A_{max} & \text{for } t_6 < t \le t_7 \end{cases} \tag{3.7}$$

$$\ddot{\theta}_{h\sin} = \begin{cases} \dfrac{A_{max}}{T_1}\left[t + \dfrac{T_1}{2\pi}\cos\left(\dfrac{2\pi}{T_1}t + \dfrac{\pi}{2}\right)\right] & \text{for } 0 \le t \le t_1 \\ A_{max} & \text{for } t_1 < t \le t_2 \\ A_{max} - \dfrac{A_{max}}{T_3}\left[(t-t_2) + \dfrac{T_3}{2\pi}\cos\left(\dfrac{2\pi}{T_3}(t-t_2) + \dfrac{\pi}{2}\right)\right] & \text{for } t_2 < t \le t_3 \\ 0 & \text{for } t_3 < t \le t_4 \\ -\dfrac{A_{max}}{T_5}\left[(t-t_4) + \dfrac{T_5}{2\pi}\cos\left(\dfrac{2\pi}{T_5}(t-t_4) + \dfrac{\pi}{2}\right)\right] & \text{for } t_4 < t \le t_5 \\ -A_{max} & \text{for } t_5 < t \le t_6 \\ -A_{max} + \dfrac{A_{max}}{T_7}\left[(t-t_6) + \dfrac{T_7}{2\pi}\cos\left(\dfrac{2\pi}{T_7}(t-t_6) + \dfrac{\pi}{2}\right)\right] & \text{for } t_6 < t \le t_7 \end{cases} \tag{3.8}$$

$$\ddot{\theta}_{p\sin} = \begin{cases} \dfrac{A_{max}}{2}\left[1 - \cos\left(\dfrac{\pi}{T_1}t\right)\right] & \text{for } 0 \le t \le t_1 \\ A_{max} & \text{for } t_1 < t \le t_2 \\ \dfrac{A_{max}}{2}\left[1 + \cos\left(\dfrac{\pi}{T_3}(t-t_2)\right)\right] & \text{for } t_2 < t \le t_3 \\ 0 & \text{for } t_3 < t \le t_4 \\ -\dfrac{A_{max}}{2}\left[1 - \cos\left(\dfrac{\pi}{T_5}(t-t_4)\right)\right] & \text{for } t_4 < t \le t_5 \\ -A_{max} & \text{for } t_5 < t \le t_6 \\ -\dfrac{A_{max}}{2}\left[1 + \cos\left(\dfrac{\pi}{T_7}(t-t_6)\right)\right] & \text{for } t_6 < t \le t_7 \end{cases} \tag{3.9}$$

$$
\dot{\theta}_s = \begin{cases}
A_{max}\dfrac{t^2}{2T_1} & \text{for } 0 \le t \le t_1 \\
V_1 + A_{max}(t - t_1) & \text{for } t_1 < t \le t_2 \\
V_2 + A_{max}(t - t_2) - A_{max}\dfrac{(t - t_2)^2}{2T_3} & \text{for } t_2 < t \le t_3 \\
V_{max} & \text{for } t_3 < t \le t_4 \\
V_{max} - A_{max}\dfrac{\left(t - t_4\right)^2}{2T_5} & \text{for } t_4 < t \le t_5 \\
V_5 - A_{max}(t - t_5) & \text{for } t_5 < t \le t_6 \\
V_6 - A_{max}(t - t_6) + A_{max}\dfrac{(t - t_6)^2}{2T_7} & \text{for } t_6 < t \le t_7
\end{cases} \tag{3.10}
$$

$$
\dot{\theta}_{hsin} = \begin{cases}
\dfrac{A_{max}}{T_1}\left[\dfrac{t^2}{2} + \left(\dfrac{T_1}{2\pi}\right)^2 \sin\left(\dfrac{2\pi}{T_1}t + \dfrac{\pi}{2}\right) - \left(\dfrac{T_1}{2\pi}\right)^2\right] & 0 \le t \le t_1 \\
V_1 + A_{max}(t - t_1) & t_1 < t \le t_2 \\
v_{@t2} & t_2 < t \le t_3 \\
V_{max} & t_3 < t \le t_4 \\
v_{@t4} & t_4 < t \le t_5 \\
V_5 - A_{max}(t - t_5) & t_5 < t \le t_6 \\
v_{@t6} & t_6 < t \le t_7
\end{cases}
$$

$$
v_{@t2} = V_2 + A_{max}(t - t_2) - \frac{A_{max}}{T_3}\left[\frac{(t - t_2)^2}{2} + \left(\frac{T_3}{2\pi}\right)^2 \sin\left(\frac{2\pi}{T_3}(t - t_2) + \frac{\pi}{2}\right) - \left(\frac{T_3}{2\pi}\right)^2\right]
$$

$$
v_{@t4} = V_4 - \frac{A_{max}}{T_5}\left[\frac{(t - t_4)^2}{2} + \left(\frac{T_5}{2\pi}\right)^2 \sin\left(\frac{2\pi}{T_5}(t - t_4) + \frac{\pi}{2}\right) - \left(\frac{T_5}{2\pi}\right)^2\right]
$$

$$
v_{@t6} = V_6 - A_{max}(t - t_6) + \frac{A_{max}}{T_7}\left[\frac{(t - t_6)^2}{2} + \left(\frac{T_7}{2\pi}\right)^2 \sin\left(\frac{2\pi}{T_7}(t - t_6) + \frac{\pi}{2}\right) - \left(\frac{T_7}{2\pi}\right)^2\right] \tag{3.11}
$$

The motion vectors are defined as $\mathbf{qs}_m = [T_1, T_2, T_3, T_m]$ for 3rd order polynomial S-curve motion profiles, $\mathbf{qhsin}_m = [T_1, T_2, T_3, T_m]$ for harmonic sinusoidal motion profiles and $\mathbf{qpsin}_m = [T_1, T_2, T_3, T_m]$, for pure sinusoidal motion profiles respectively. The general representation of a motion vector is defined as $\mathbf{q}_m = [T_1, T_2, T_3, T_m]$ for all motion profile types. Two motion cases were defined for two different motion times as T_m=20t1h and T_m=21t1h. t1h is the time which is half of the first natural period of the manipulator. T_1 was selected from 1t1h-5t1h for both motion cases and T_2 was selected according to acceleration time which varies from 2t1h-10t1h.

$$\dot{\theta}_{psin} = \begin{cases} \frac{A_{max}}{2}\left[t - \frac{T_1}{\pi}\sin\left(\frac{\pi}{T_1}t\right)\right] & \text{for } 0 \le t \le t_1 \\ V_1 + A_{max}(t - t_1) & \text{for } t_1 < t \le t_2 \\ V_2 + \frac{A_{max}}{2}\left[(t - t_2) + \frac{T_3}{\pi}\sin\left(\frac{\pi}{T_3}(t - t_2)\right)\right] & \text{for } t_2 < t \le t_3 \\ V_{max} & \text{for } t_3 < t \le t_4 \\ V_4 - \frac{A_{max}}{2}\left[(t - t_4) - \frac{T_5}{\pi}\sin\left(\frac{\pi}{T_5}(t - t_4)\right)\right] & \text{for } t_4 < t \le t_5 \\ V_5 - A_{max}(t - t_5) & \text{for } t_5 < t \le t_6 \\ V_6 - \frac{A_{max}}{2}\left[(t - t_6) + \frac{T_6}{\pi}\sin\left(\frac{\pi}{T_7}(t - t_6)\right)\right] & \text{for } t_6 < t \le t_7 \end{cases} \tag{3.12}$$

3.3 Modeling of Manipulator in ANSYS and Transient Analyses Calculations

The finite element model of the flexible beam was created in ANSYS and the transient response of the beam under a given velocity motion profile was calculated. BEAM type elements were used for the finite element modeling. BEAM188 element type which has two nodes was selected in order to model the flexible manipulator. BEAM188 has six degrees of freedom at each node. These include translations in the x, y, and z directions and rotations about the x, y, and z directions. BEAM188 has an internal node in the interpolation scheme, effectively making this a beam element based on quadratic shape functions. Two-point masses and their moments of inertia were included in the model for the accelerometer and payload masses. The model properties of the manipulator were given in Table 3.1.

The transient vibration response under a given motion profile can be calculated by solving the time dependent ODE given in Eq.(3.13).

$$[M]\ddot{X}+[C]\dot{X}+[K]X=F \tag{3.13}$$

Where the X matrix represents the node displacements of the elements. M, C, K and F are mass, damping, stiffness and force matrix respectively.

Table 3.1 FE model properties of the flexible manipulator

Elastic modulus / Poisson ratio	$193.6x10^6$ Pa / 0.3
Density	7760 kg/m^3
Accelerometer mass	47 gr
Inertia of the accelerometer	$9.18450x10^{-6}$ kgm^2
Payload mass	51 gr
Inertia of payload	$9.18450x10^{-6}$ kgm^2
Cross section	2x39.4 mm^2
Beam length (L_2)	352 mm
Acc. and Payload Position from the origin	322 mm
Rayleigh damping coefficients	η=0 and $\beta=3.75x10^{-5}$
Motor rotational spring constant	16000 Nm/rad
Element size	2 mm
Time step	Δt=0.005 s

The mass and stiffness matrices can be calculated using the mechanical and physical properties of the manipulator. The damping matrix was calculated by using Rayleigh damping coefficients which were calculated using the damping ratio of experimental results and natural frequency of the manipulator. The dynamic response of the manipulator is calculated numerically by using the Newmark method (Karagülle et al., 2017; Newmark, 1959) in ANSYS under a given motion profile. The natural frequencies of the simulation and experiment are fn_{sim}=8.3319 Hz and fn_{exp}=8.3313 Hz.

3.4 Experimental Setup and Data Logging

A 200 W HCKFS-23B Mitsubishi Servo motor with a harmonic drive reductor Model HFUC-32-100/100 which has 1:100 ratio was used to rotate the flexible manipulator. The model parameters of the flexible manipulator were given in Table 3.1. An ADLINK PCI-8253 Analog Motion Controller Board was used to send voltage to the motor driver and actuate the flexible manipulator. Time and velocity vectors were sent via this analog motion controller board to the servo motor driver. A Laser displacement sensor Keyence LK-G157 was used to observe and measure the vibrations of a point on the flexible manipulator during the motion. The analog output of the displacement sensor was read and saved with a 1 kHz sampling rate by using a NI DAQPad-6015 data acquisition module in LabVIEW. A laser displacement sensor was placed on the output of the harmonic drive reductor by using a rigid aluminum profile which makes an angle of 90° with the flexible manipulator as shown in Figure 3.2 (a). The other needed equipment are a PC, NI DAQPad-6015, Mitsubishi Servo Motor Driver MR-J2(S)-20A, and a display panel Keyence LK-G3001, shown in Figure 3.2 (b) during the measurement process.

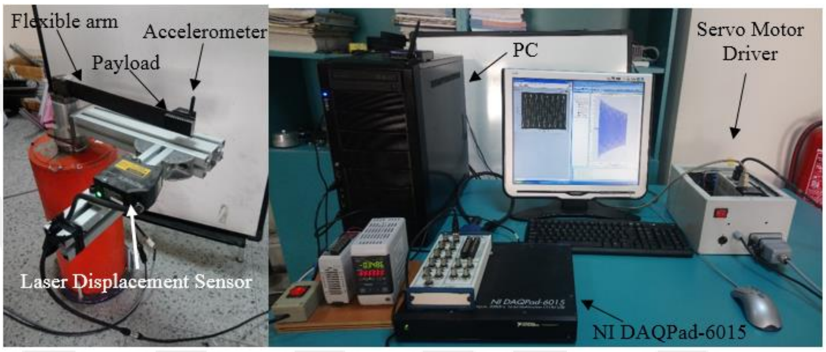

(a) (b)

Figure 3.2 Experimental setup (a) Flexible manipulator, laser displacement sensor (b) PC, NI DAQPad-6015, Servo Driver, Sensor Display Panel

The measured first natural frequencies were 8.3313 Hz and 8.1719 Hz according to the displacement sensor and accelerometer sensor data respectively. The transient and residual vibration response of the manipulator under a given motion profile showed that the natural frequency calculated and measured by using displacement sensor data was the real frequency of the system. Therefore 8.3313 Hz was used to define the motion profiles and time parameters. The fundamental natural period of the system was calculated to be approximately $T_n \approx 0.12$ sec.

3.5 Results and Discussions

In this part, some of the obtained transient and residual vibrations results were graphically presented to compare the experimental results to the ANSYS simulations. Afterwards, all the experiment results were given in tabular format. The maximum residual vibration amplitudes were shown in 3D graphics in terms of T_1, T_2 and amplitudes.

The comparison of some of the simulation and experimental results are shown in Figure 3.5, Figure 3.4 and Figure 3.5. The 3rd order S-curve velocity motion profile results are shown in Figure 3.5 (a) and (b). The results of harmonic and pure sinus velocity motion profiles are shown in Figure 3.4 and Figure 3.5 respectively for different motion cases. It was observed from Figure 3.5, Figure 3.4 and Figure 3.5 that the analysis results of the ANSYS model are in good agreement with the experimental results. This proves that the established model is consistent with the experimental setup. The observed maximum transient and residual vibration amplitudes for both the experimental and the simulation results were shown in Table 3.2 and Table 3.3 in detail. While the results of motion cases for T_m=20t1h were shown in Table 3.2, Table 3.3 includes the results of motion cases for T_m=21t1h. The maximum residual vibration amplitudes were shown in Figure 3.6 by using 3 axis graphics in terms of T_1, T_2 and amplitudes in order to see clearly the effect of the time parameters on the residual vibration amplitudes for each value T_m.

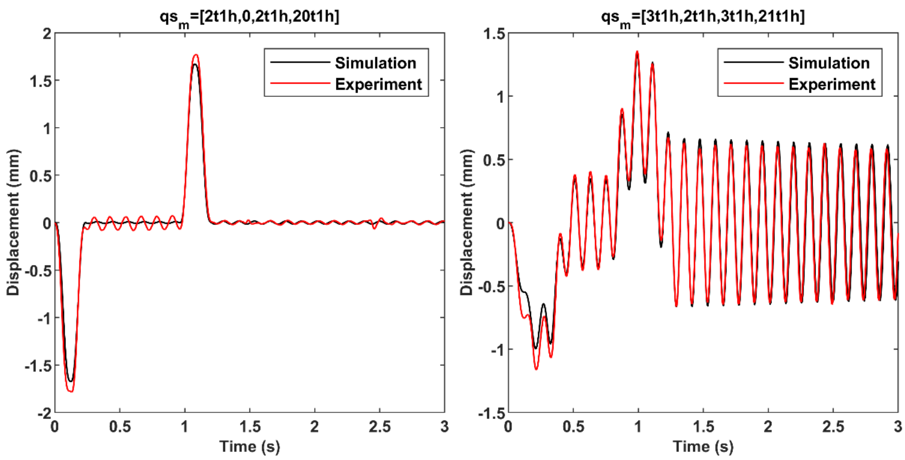

(a) (b)

Figure 3.3 The results of the 3rd order S-curve velocity motion profiles for two motion cases

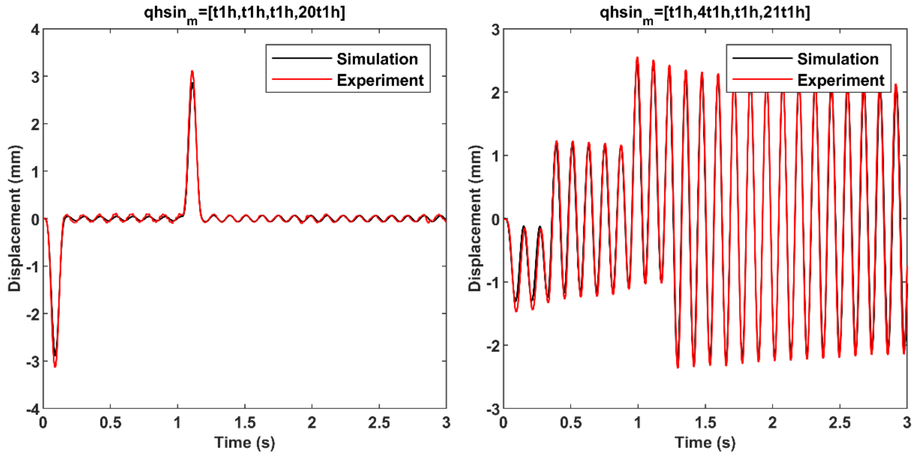

(a) (b)

Figure 3.4 The results of the harmonic sinus velocity motion profiles for two motion cases

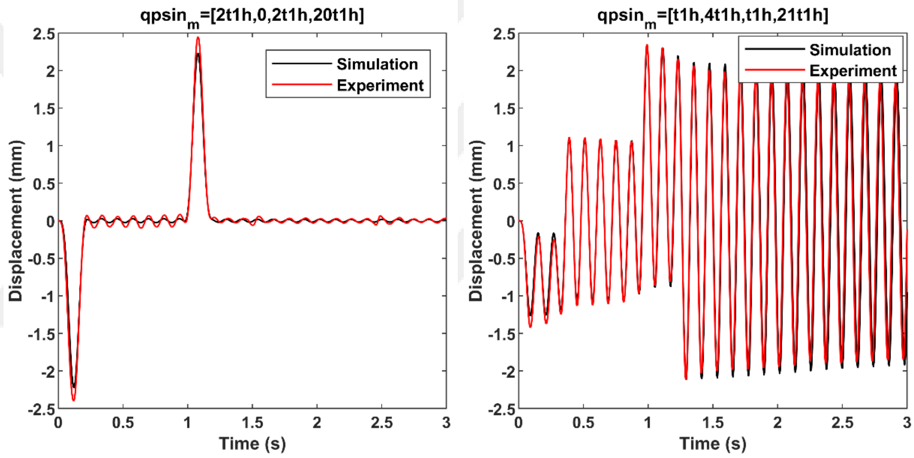

(a) (b)

Figure 3.5 The results of the pure sinus velocity motion profiles for two motion cases

According to the results given in Table 3.2, Table 3.3 , the effect of the time parameters on residual vibrations for all motion profiles can be explained as follows;

- When T_m=20t1h or T_m=21t1h, S-curve motion profile results were sensitive and reached high values for both T_1 values which were odd multiples of t1h and T_2 values which were even multiples of t1h. When T_1 and T_2 values were selected as even multiples of t1h, the amplitudes of residual vibration were very low.

- When T_m=20t1h, harmonic sinus motion profile residual vibration amplitudes were sensitive and reached high values for both T_1 values which were selected as 2t1h, and T_2 values which were odd multiples of t1h. If T_m=21t1h, the residual vibration amplitudes reached high values for both T_1 values which were selected as t1h and T_2 values which were even multiples of t1h. If T_1 was selected as 3t1h for T_m=20t1h, the observed residual vibration amplitudes were very low. When T_1 and T_2 values were selected as odd multiples of t1h, the residual vibration amplitudes reached very low values for both T_m values.

- When T_m=20t1h, pure sinus motion profile residual vibration amplitudes were sensitive and reached high values for both T_1 values which were selected as even multiples of t1h and T_2 values which were odd multiples of t1h. The residual vibration amplitudes reached high values for both T_1 values which were selected as t1h and T_2 values which were even multiples of t1h for both T_m=20t1h and T_m=21t1h. When T_1 and T_2 values were selected as odd multiples of t1h, the residual vibration amplitudes reached very low values for both T_m values.

Table 3.2 The simulation and experiment results for T_m=20t1h in terms of maximum transient and residual amplitudes

	Simulation						**Experiment**					
	Max. Transient Ampl. (mm)			Max. Residual Ampl. (μm)			Max. Transient Ampl. (mm)			Max. Residual Ampl. (μm)		
Motion case	**qs**$_m$	**qhsin**$_m$	**qpsin**$_m$	**qs**$_m$	**qhsin**$_m$	**qpsin**$_m$	**qs**$_m$	**qhsin**$_m$	**qpsin**$_m$	**qs**$_m$	**qhsin**$_m$	**qpsin**$_m$
[t1h, 0, t1h, T_m]	4.59	5.296	5.087	877.28	1166.3	1080	4.71	5.672	5.364	706.65	921.1	833.2
[t1h, t1h, t1h, T_m]	2.558	2.885	2.787	50.212	67.243	62.194	2.842	3.144	3.043	72.7	92.65	64.33
[t1h, 2t1h, t1h, T_m]	1.812	2.043	1.974	292.59	389.04	360.25	1.905	2.218	2.166	296.3	291.8	339.4
[t1h, 3t1h, t1h, T_m]	1.449	1.634	1.579	61.174	80.243	74.394	1.597	1.8	1.74	63.935	87.8	58.7
[t1h, 4t1h, t1h, T_m]	1.242	1.401	1.353	176.48	233.5	216.28	1.352	1.572	1.499	167.85	214.5	201.15
[t1h, 5t1h, t1h, T_m]	1.115	1.257	1.215	69.8	91.543	84.84	1.32	1.327	1.279	73.075	91.4	86.695
[t1h, 6t1h, t1h, T_m]	1.035	1.167	1.128	125.98	166.78	155.09	1.239	1.23	1.297	116.35	205.2	166.35
[t1h, 7t1h, t1h, T_m]	0.988	1.114	1.077	81.625	107.58	99.498	1.082	1.174	1.219	87.62	112	101.745
[t1h, 8t1h, t1h, T_m]	0.966	1.09	1.053	98.722	130.19	120.61	1.116	1.169	1.175	92.275	158.4	118.3
[2t1h, 0, 2t1h, T_m]	1.673	2.503	2.226	15.835	19.299	19.704	1.77	2.774	2.448	20.38	54.04	29.03
[2t1h, t1h, 2t1h, T_m]	1.197	2.88	2.319	26.005	2262.2	1516.8	1.326	3.016	2.453	36.115	2314	1564.5
[2t1h, 2t1h, 2t1h, T_m]	0.96	1.438	1.28	6.236	6.675	7.093	1.131	1.588	1.451	41.255	21.37	41.425
[2t1h, 3t1h, 2t1h, T_m]	0.823	2.003	1.61	13.593	1562.7	1049	0.96	2.115	1.721	30.67	1578	1082
[2t1h, 4t1h, 2t1h, T_m]	0.747	1.122	0.997	2.707	3.358	1.886	0.874	1.259	1.147	16.015	56.93	28.505
[2t1h, 5t1h, 2t1h, T_m]	0.695	1.7	1.365	11.843	1318.4	882.48	0.883	1.833	1.426	31.195	1333	876.95
[2t1h, 6t1h, 2t1h, T_m]	0.672	1.011	0.898	5.193	3.506	2.705	0.8695	1.123	1.021	17.005	14.09	22.67
[3t1h, 0, 3t1h, T_m]	1.491	1.481	1.275	97.949	80.303	5.81	1.691	1.628	1.463	112.6	105.1	21.305
[3t1h, t1h, 3t1h, T_m]	1.244	1.196	1.029	23.664	22.351	9.032	1.332	1.385	1.234	47.25	82.44	28
[3t1h, 2t1h, 3t1h, T_m]	1.079	1.036	0.891	56.545	49.596	11.385	1.12	1.151	1.092	66.665	87.47	17.83
[3t1h, 3t1h, 3t1h, T_m]	0.982	0.942	0.81	27.827	26.225	11.349	1.05	1.12	0.9805	41.295	47.03	15.655
[3t1h, 4t1h, 3t1h, T_m]	0.925	0.888	0.763	39.812	36.116	10.275	1.08	1.115	0.9558	55.695	52	13.295
[4t1h, 0, 4t1h, T_m]	1.115	1.115	1.185	11.349	11.066	11.285	1.34	1.335	1.343	14.4	35.38	27.08
[4t1h, t1h, 4t1h, T_m]	0.983	0.973	1.161	15.395	9.014	249.35	1.081	1.119	1.314	28.265	58.96	253.15
[4t1h, 2t1h, 4t1h, T_m]	0.896	0.894	0.951	4.308	3.82	3.475	1.076	1.074	1.08	26.045	46.34	11.3115
[5t1h, 0, 5t1h, T_m]	1.179	1.092	1.07	34.773	9.218	4.753	1.33	1.211	1.272	39.985	17.69	28.67

Table 3.3 The simulation and experiment results for T_m=21t1h in terms of maximum transient and residual amplitudes

	Simulation						Experiment					
	Max. Transient Ampl. (mm)			Max. Residual Ampl. (μm)			Max. Transient Ampl. (mm)			Max. Residual Ampl. (μm)		
Motion case	**qs_m**	**$qhsin_m$**	**$qpsin_m$**	**qs_m**	**$qhsin_m$**	**$qpsin_m$**	**qs_m**	**$qhsin_m$**	**$qpsin_m$**	**qs_m**	**$qhsin_m$**	**$qpsin_m$**
[t1h, 0, t1h, T_m]	7.305	9.245	8.665	6770.3	9001	8337.88	7.561	9.471	8.789	6911	9174	8385
[t1h, t1h, t1h, T_m]	2.429	2.742	2.649	19.11	19.542	19.341	2.609	3.046	2.861	18.085	39.38	35.755
[t1h, 2t1h, t1h, T_m]	2.939	3.566	3.379	2525.8	3355.82	3108.46	3.077	3.745	3.572	2537	3445.5	3218.5
[t1h, 3t1h, t1h, T_m]	1.374	1.552	1.499	4.991	8.13	7.634	1.54	1.704	1.616	39.83	26.625	33.74
[t1h, 4t1h, t1h, T_m]	2.007	2.435	2.307	1715.1	2279.28	2110.81	2.165	2.558	2.348	1806.5	2360	2090.5
[t1h, 5t1h, t1h, T_m]	1.05	1.186	1.145	5.0313	6.603	6.047	1.185	1.347	1.281	44.605	37.65	27.98
[t1h, 6t1h, t1h, T_m]	1.665	2.022	1.915	1414.1	1879.85	1740.75	1.717	2.165	2.01	1418	1997	1777
[t1h, 7t1h, t1h, T_m]	0.921	1.039	1.004	5.74	5.014	5.525	1.066	1.129	1.129	31.835	11.084	26.85
[t1h, 8t1h, t1h, T_m]	1.539	1.873	1.774	1300.9	1733.21	1605.26	1.57	2.025	1.859	1309.5	1802	1.5575
[2t1h, 0, 2t1h, T_m]	1.574	2.347	2.09	1.395	39.212	25.759	1.85	2.575	2.274	44.26	45.37	54.595
[2t1h, t1h, 2t1h, T_m]	1.115	1.662	1.48	8.2525	229.968	155.573	1.342	1.738	1.556	30.915	190.8	153.25
[2t1h, 2t1h, 2t1h, T_m]	0.891	1.329	1.183	11.399	49.185	33.718	1.151	1.455	1.412	40.415	50.1	39.42
[2t1h, 3t1h, 2t1h, T_m]	0.764	1.139	1.014	10.539	138.968	94.0273	0.9594	1.258	1.082	29.925	131.75	100.425
[2t1h, 4t1h, 2t1h, T_m]	0.685	1.023	0.91	8.214	55.754	38.538	0.851	1.141	1.058	13.355	56.04	46.625
[2t1h, 5t1h, 2t1h, T_m]	0.636	0.95	0.845	6.261	99.475	68.127	0.7567	1.161	0.9663	38.925	93.005	70.65
[2t1h, 6t1h, 2t1h, T_m]	0.608	0.906	0.807	4.351	64.788	44.241	0.7514	1.023	0.945	40.595	86.685	56.415
[3t1h, 0, 3t1h, T_m]	1.828	1.763	1.192	956.4	778.561	19.285	1.846	1.79	1.319	944.25	799.2	54.875
[3t1h, t1h, 3t1h, T_m]	1.156	1.118	0.955	5.4347	6.305	6.235	1.287	1.295	1.157	44.315	47.51	43.725
[3t1h, 2t1h, 3t1h, T_m]	1.325	1.219	0.822	663.34	538.865	8.105	1.356	1.354	0.98	646.4	564.65	43.78
[3t1h, 3t1h, 3t1h, T_m]	0.899	0.873	0.745	6.084	1.304	2.683	1.076	0.9828	0.9428	45.755	33.47	24.87
[3t1h, 4t1h, 3t1h, T_m]	1.121	1.033	0.694	559.37	452.807	7.722	1.201	1.1	0.8474	555.8	444.6	42.66
[4t1h, 0, 4t1h, T_m]	1.032	1.029	1.095	7.0625	8.837	10.972	1.173	1.189	1.259	31.995	48.55	14.63
[4t1h, t1h, 4t1h, T_m]	0.896	0.892	0.951	9.58	11.177	19.559	1.11	1.049	1.117	46.34	34.53	37.67
[4t1h, 2t1h, 4t1h, T_m]	0.815	0.81	0.866	10.133	11.177	13.203	0.9026	1.006	1.011	44.72	37.28	30.31
[5t1h, 0, 5t1h, T_m]	1.287	1.041	0.972	467.3	91.712	8.298	1.366	1.181	1.153	517.8	94.4	40.395

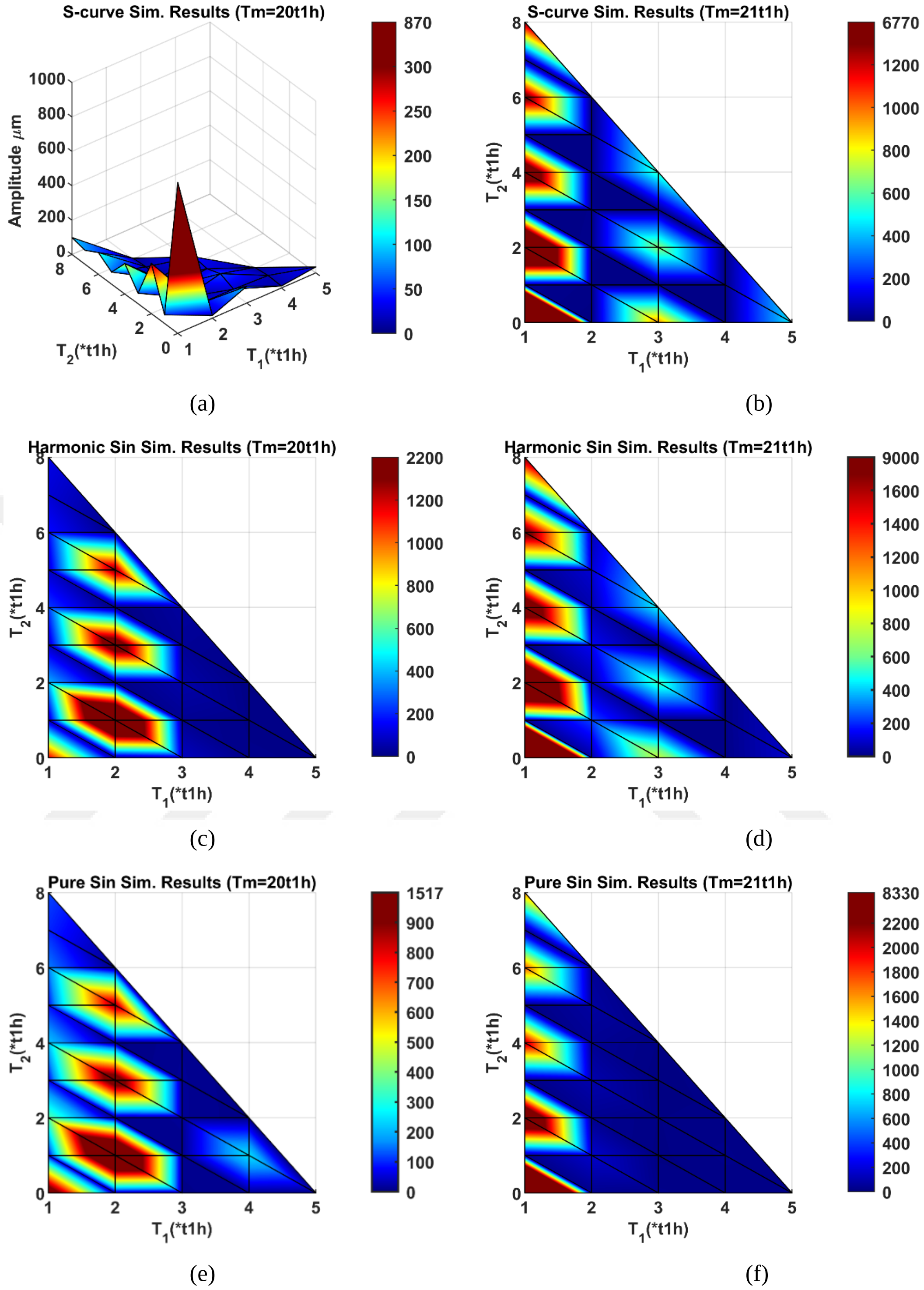

Figure 3.6 Residual vibration results for all cases and motion profile types

3.6 Sensitivity Analyses of the Motion Profiles

According to the obtained results, it has been observed that the vibration results are extremely affected by T_1, T_2 and T_m at certain values for the 3rd order polynomial and the sinusoidal motion profiles. In such cases, it is important that the natural frequency is measured correctly. Otherwise, the calculation of the time parameters and motion profile definition would be wrong. Therefore, expected vibration results cannot be achieved. In this study two sensors were used to obtain the natural frequency of the system. As mentioned in section 3.4 two different natural frequencies were obtained by using the measured data from both the displacement sensor and the accelerometer. Then it was realized that the correct natural frequency is obtained from the displacement sensor. There was a 2% error in the measurement of the accelerometer. Therefore, some simulations were performed to observe the sensitivity of all motion profiles to any measurement error in the range of 0% to 4% during the natural frequency measurement of the manipulator. Two different motion profile vectors were selected. These are $\mathbf{q}_m$=[2t1h, 4t1h, 2t1h, 20t1h] and $\mathbf{q}_m$=[3t1h, 3t1h, 3t1h, 21t1h]. T_n (natural period) values were assumed as ranging from 0.121 sec to 0.125 sec with increment of 0.001 sec. After performing the simulations, differences in maximum residual vibration amplitudes between the original T_n and assumed T_n values were shown in (a) and (b) in terms of %error.

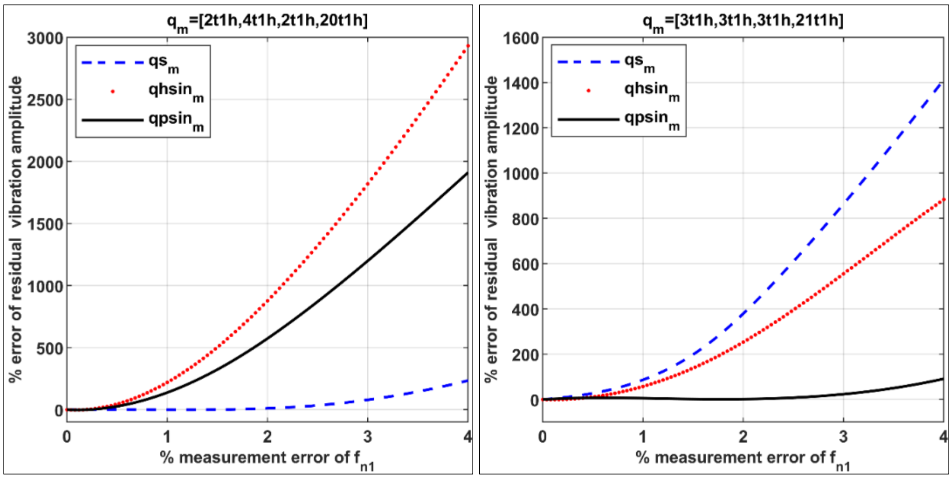

(a) (b)

Figure 3.7 Sensitivity analyses results (a) for $\mathbf{q}_m$=[2t1h, 4t1h, 2t1h, 20t1h] (b) for $\mathbf{q}_m$=[3t1h, 3t1h, 3t1h, 21t1h]

While the polynomial S-curve motion profile results were less sensitive than sinusoidal motion profiles for motion case $\mathbf{q}_m$=[2t1h, 4t1h, 2t1h, 20t1h], sinusoidal ones caused less error than polynomial motion profile for motion case $\mathbf{q}_m$=[3t1h, 3t1h, 3t1h, 21t1h]. For this reason, as a precaution against a possible measurement error, if T_1 and T_m were selected as 2t1h and (2n)t1h ($n \in \mathbb{N}$) respectively, the polynomial S-curve motion profiles should be preferred. Otherwise if T_1 and T_m were selected as 3t1h and (2n+1)t1h ($n \in \mathbb{N}$) respectively pure sinusoidal motion profile should be selected.

3.6 Conclusions

In this part of the study, the effect of three different velocity motion profiles with seven segments on the end point transient and residual vibrations of a flexible manipulator were investigated experimentally and by performing finite element simulations with ANSYS. These motion profiles were 3rd order polynomial S-curve and two different trigonometric (harmonic and pure sinusoidal) S-curve motion profiles. Symmetrical velocity motion profiles were used, and the time parameters of the motion profiles were chosen using either half-integer multiples or integer multiples of the fundamental period. The experimental results were compared with the transient analysis results obtained with ANSYS. The effects of the time parameters of all motion profiles on endpoint vibrations were investigated by comparing them in terms of amplitudes.

As a result of the performed studies, it has been shown that the selection of the time parameters as an integer multiple of the fundamental period is effective in reducing residual vibration amplitudes to almost zero for 3rd order polynomial S-curve motion profiles. The time parameters of trigonometric profiles (harmonic and pure sinusoidal) should be selected as half integer multiples of the fundamental period of the manipulator to obtain almost zero residual vibrations.

The sensitivity of all motion profiles to any measurement error in the range of 0% to 4% during the natural frequency measurement of the manipulator was also shown.

The polynomial S-curve motion profile results were less sensitive than the sinusoidal motion profiles for motion case $\mathbf{q}_m$=[2t1h, 4t1h, 2t1h, 20t1h], while the sinusoidal ones caused less error than the polynomial motion profile for motion case $\mathbf{q}_m$=[3t1h, 3t1h, 3t1h, 21t1h]. For this reason, as a precaution against a possible measurement error if T_1 and T_m were selected as 2t1h and (2n)t1h ($n \in \mathbb{N}$) respectively, the polynomial S-curve motion profiles should be preferred. Otherwise if T_1 and T_m were selected as 3t1h and (2n+1)t1h ($n \in \mathbb{N}$) respectively, a pure sinusoidal motion profile should be preferred.

CHAPTER FOUR
VIBRATION CONTROL OF A FLEXIBLE MANIPULATOR BY ACTIVE CABLE TENSION

4.1 Methodology

In this part of the study, firstly the finite element of the flexible manipulator to which cables were attached was modeled in ANSYS. The cables were subjected to four different initial strain conditions, including no prestrain and three different values. The modal analyses were performed for different pretension values on the cables. The open loop and closed loop control simulations were performed using the trapezoidal motion profiles. The end point vibration amplitudes, axial forces of the cables, and the bending strain values of one element near the fixed end were observed in order to define the limitations of the sensors and actuators which will be selected for experimental setup.

According to the obtained results, the experimental setup was designed and manufactured. The design was revised two times due to both the reductor replacement and the mini load cell installation.

The closed loop control of the experimental setup was performed for both the transient and residual regions in ANSYS. The first natural frequency of the system was too high for the selected control actuator, therefore the length of the flexible manipulator and the diameter of the pulley which is connected to the control actuator were changed in order to decrease the natural frequency of the system. The closed loop control was performed with velocity feedback control.

4.2 Finite Element Model of Flexible Beam with Cables ANSYS APDL

The finite element model of the flexible beam with cables was established in Ansys Mechanical APDL instead of Ansys Workbench in order to perform the closed loop control simulations by writing scripts. The flexible beam was modeled by using

BEAM188 element and the cables were modeled by using LINK180 element. LINK180 elements were used to model the cables by turning off the compression capacity of the element, thus simulating members that carry only axial tension forces. Detailed schematic view of the model is shown in Figure 4.1 (a). The model parameters are given in Table 4.1 and established model in Ansys is shown in Figure 4.1 (b).

The characterizing parameters of the symmetric trapezoidal motion profile are acceleration and deceleration times, and they were defined as percentages of the total motion time. The manipulator was rotated by 90˚ in 1 second. The motion vector of trapezoidal motion profiles was defined as $\mathbf{q_m}$=[T_{acc}-T_{dec}-T_m]. The acceleration time T_{acc} and deceleration time T_{dec} values were defined in tables and figures as %T_m.

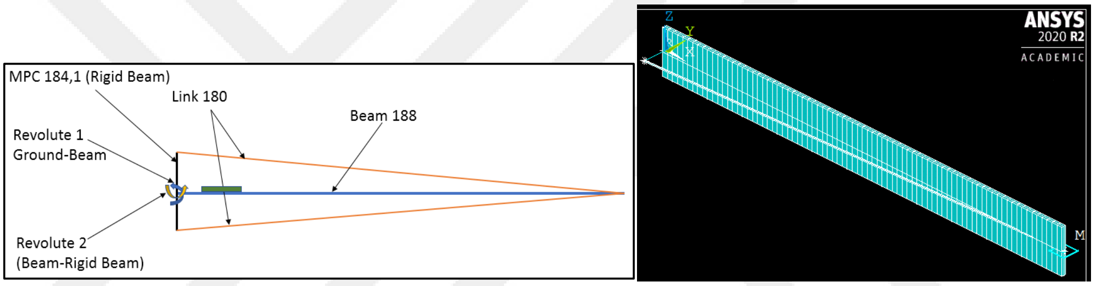

(a) (b)

Figure 4.1 (a) Schematic FE model of tendon controlled flexible beam (b) FE model in Ansys

Table 4.1 Model parameters

Elastic modulus	$2x10^{11}$ Pa
Poisson ratio	0.3
Density	7850 kg/m^3
Payload mass	1.25 kg
Inertia of payload	$633.445x10^{-6}$ kgm^2
Cable Diameter	Ø1 mm
Cross section	3.8x40 mm^2
Beam length (L_2)	400 mm
Rayleigh damping coefficients	η=0 and β=$3.75x10^{-5}$
Motor rotational spring constant	K_{m2}=16000 Nm/rad
Number of finite elements	ne2=80
Time step	Δt=0.005 s

4.3 The effect of the Cable Pretension on Natural Frequencies and Amplitudes

The natural frequencies obtained from both modal analyses and fast Fourier transform by using free vibration responses are shown in Table 4.2. The reason of the differences between the modal analyses and fast Fourier transform frequency result is that both cables were not effective at the same time on the stiffness matrix. This situation was understood from the observation of the axial forces on the cables during the motion as shown in Figure 4.2.

Table 4.2 First natural frequencies

		Trapezoidal Motion Cases				
Pretension	Modal Analyses	**[0.1-0.1-1]**	**[0.2-0.2-1]**	**[0.3-0.3-1]**	**[0.4-0.4-1]**	**[0.5-0.5-1]**
No cable	5.5786 Hz	5.5786	5.5786	5.5786	5.5786	5.5786
0	7.9992 Hz	6.9316	6.8777	6.9794	6.9628	6.9134
5N	8.0279 Hz	6.9128	6.9466	7.7108	7.1592	6.9994
10N	8.0564 Hz	6.9319	7.0433	7.4993	7.3843	7.0978
15N	8.0848Hz	6.9504	7.1987	7.4894	7.9754	7.2699

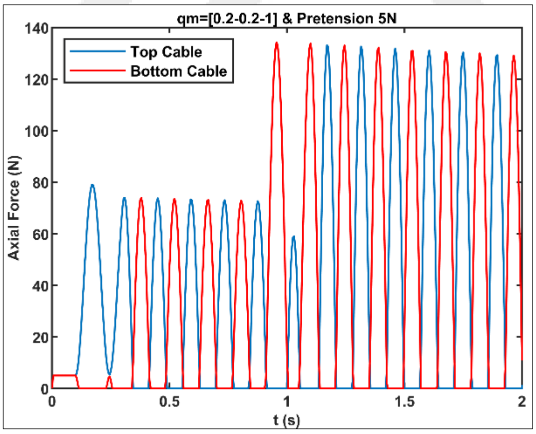

Figure 4.2 Axial forces on the cables during the $\mathbf{q_m}$=[0.2-0.2-1] with 5N pretension

The effect of the value of pretension on the vibration results for both $\mathbf{q_m}$=[0.3-0.3-1] and $\mathbf{q_m}$=[0.4-0.4-1] for all pretension values and without cable model are shown in (a) and (b). It was observed that the vibration amplitudes are not directly affected by the value of pretension on cables, rather they are related to the natural period and the parameters of the motion profile. It was previously established in Chapters Two and

Three, that coinciding or close values of the first natural period of the manipulator and the deceleration time of the motion profile reduce the vibration amplitudes.

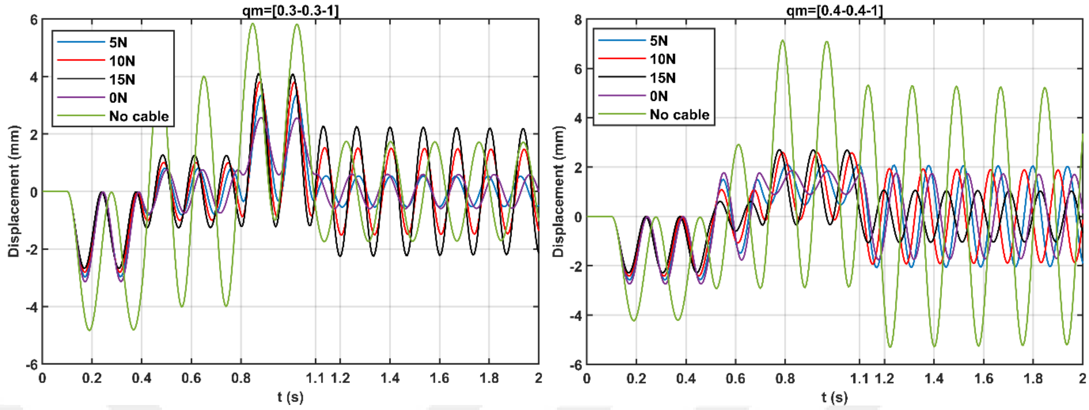

(a) (b)

Figure 4.3 The effect of the pretension values on the vibration amplitudes

4.4 The Determination of the System Limitations

There should be a limitation for the initial pretension. Two parameters were taken into consideration. During the motion, the axial force on the cables should not reach the yield force, and the axial force of the cable should not cause buckling failure of the beam. For this reason, the axial yield force (Fax_{yield}) and the maximum axial load (P_{crt}) that the beam can carry was calculated from Eq. (4.1) and Eq. (4.2), respectively. During the motion, these values were monitored. The maximum obtained Fax_{yield} on cables was also used for the calculation of the needed torque amount of control motor. According to the obtained results that are shown in Table 4.3 and Table 4.4 the maximum Fax (axial force) is 208.9676 N, and it was reached for 15N pretension and $\mathbf{q_m}$=[0.1-0.1-1]. However, this value is higher than Fax_{yield}. Therefore, if a pretension of 15N is going to be used, motion case $\mathbf{q_m}$=[0.1-0.1-1] should not be chosen. 15 N pretension is safe to be used, if the diameter of the cable increased, so that Fax is less than Fax_{yield}. The maximum holding torque that was obtained is 4.179352Nm. This can be taken as a reference for the selection of the control motor.

$$\begin{gathered} Fax_{yield} = \sigma_{yield} A_{cable} \rightarrow \sigma_{yield} = 250\text{ MPa}, A_{cable} = \pi(0.5x10^{-3})^2 \\ Fax_{yield} = 196.35\text{ N} \end{gathered} \tag{4.1}$$

$$P_{crt} = \frac{\pi^2 EI}{L_e^{\ 2}} \rightarrow L_e = 2L \rightarrow P_{crt} = 564 \text{ N} \tag{4.2}$$

Table 4.3 Axial Forces on Cable 1 for Open Loop Control

	Trapezoidal Motion Cases/CableTension1 (N)				
Pretension	**[0.1-0.1-1]**	**[0.2-0.2-1]**	**[0.3-0.3-1]**	**[0.4-0.4-1]**	**[0.5-0.5-1]**
5N	161.5214	133.1011	60.7261	53.3922	97.4236
10N	186.3857	119.3072	62.7435	55.4848	94.5357
15N	205.5897	98.3538	65.0928	57.945	83.83

Table 4.4 Axial Forces on Cable 2 for Open Loop Control

	Trapezoidal Motion Cases/CableTension2 (N)				
Pretension	**[0.1-0.1-1]**	**[0.2-0.2-1]**	**[0.3-0.3-1]**	**[0.4-0.4-1]**	**[0.5-0.5-1]**
5N	162.0161	134.2044	67.7446	44.6053	98.7319
10N	187.1463	122.4846	81.1568	58.7313	98.3083
15N	208.9676	109.608	91.2579	65.5933	94.4689
Pretension	**Needed Holding Torque (Nm)**				
5N	3.240322	2.684088	1.354892	0.892106	1.974638
10N	3.742926	2.449692	1.623136	1.174626	1.966166
15N	4.179352	2.19216	1.825158	1.311866	1.889378

4.5 Open Loop and Closed Loop Control Results on Simulation

In Ansys APDL closed loop control algorithm that includes proportional control (K_p) was established by a written script. The bending strain value on the element which is 15 mm away from the fixed end was read from the simulation and used as feedback for the closed loop control. The results obtained from the closed loop control for different K_p values and different motion profiles are shown in Figure 4.4.

The closed loop simulations were also studied using different motion profiles. The end point vibrations were suppressed significantly using only proportional controller and the vibration control was successfully performed.

According to the open loop results, maximum vibration amplitudes were obtained for case $\mathbf{q_m}$=[0.1-0.1-1]. The bending strain values of motion case $\mathbf{q_m}$=[0.1-0.1-1] were taken as a reference for strain gauges selection limits. According to the obtain bending strain values the maximum limit was $3x10^{-4}$ m/m as shown in Figure 4.5.

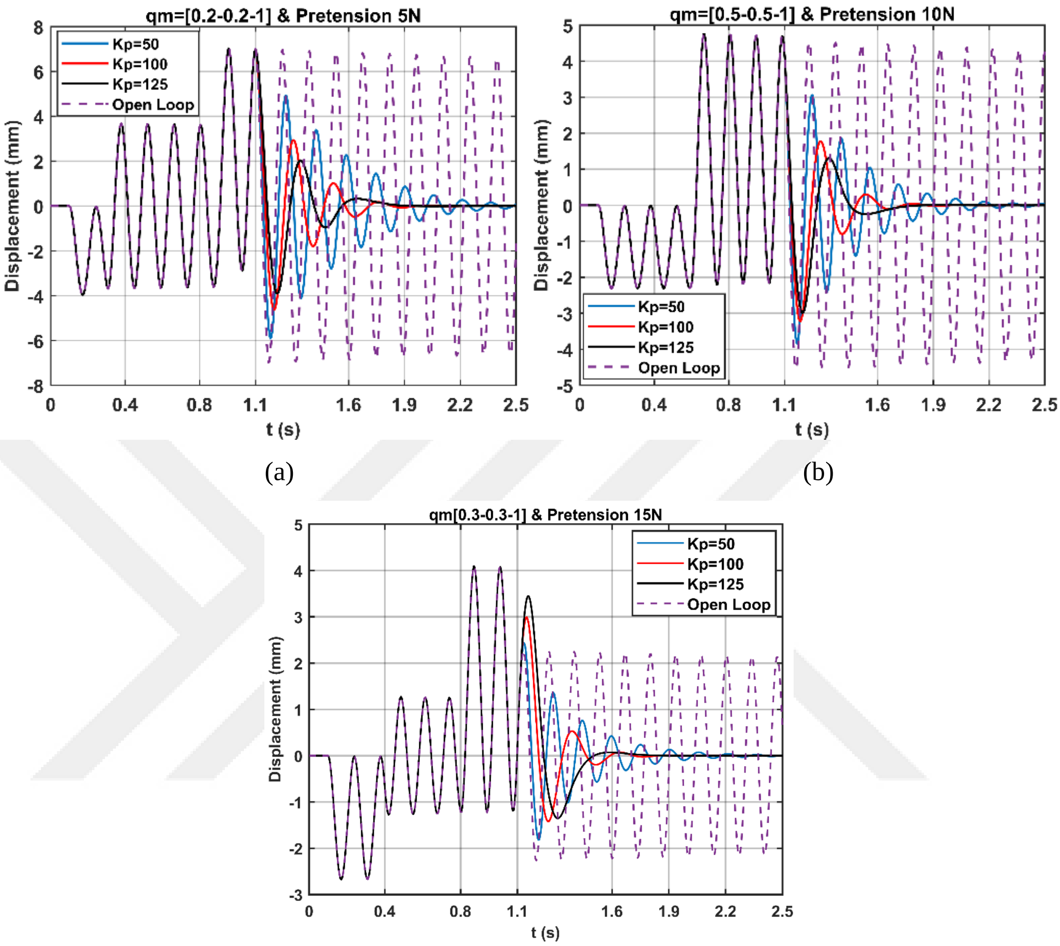

(a) (b)

(c)

Figure 4.4 Closed Loop Control for Different Kp values for same Pretension Axial Load

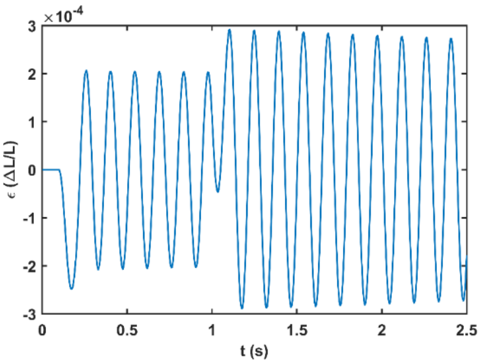

Figure 4.5 Bending strain values during motion

4.6 Experimental Setup Design and Production

The main purpose of the design procedure was to connect the cables to the center of the cross section of the flexible manipulator. In order to achieve this purpose, the control motor should be behind the main rotation axis of the flexible manipulator. A 200W Servo Motor was planned to be used as the control motor with an APEX reductor that has a 1:10 reduction ratio. A pulley of 70 mm diameter was designed to connect the cables on it. The diameter of the pulley was chosen as small as possible, due to the dimension constraints of the other parts. The setup was designed in compliance with these constrains in mind and is shown in Figure 4.6.

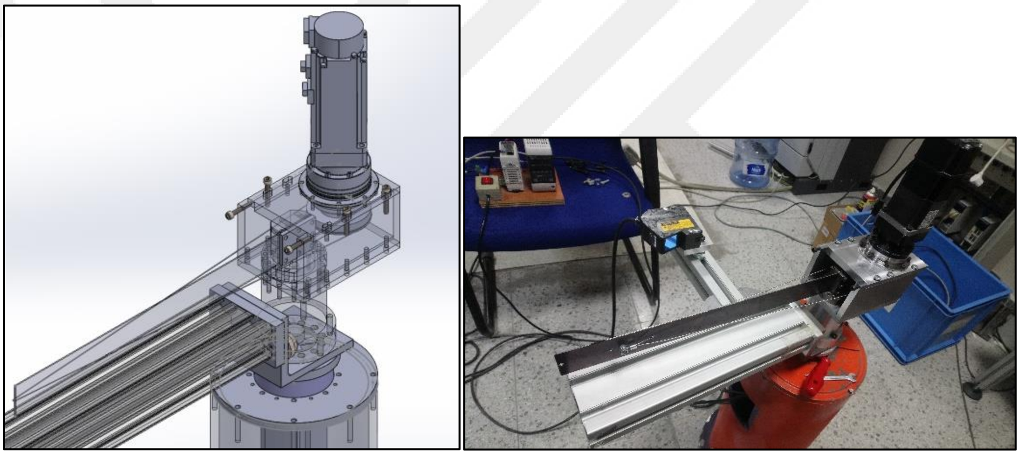

(a) (b)

Figure 4.6 a) SolidWorks Model b) Manufactured Setup

4.7 Open Loop Experimental Results

In this part, it was attempted to create the FE model of the experimental setup. The finite element model of the flexible beam with cables was established in Ansys Mechanical APDL. The model was created step by step. Firstly, only the manipulator was modeled, and the first natural frequency was obtained by performing modal analyzes. The frequency obtained from the simulation was compared with the frequency obtained experimentally. Then the payload was added, and again the natural frequencies were compared. The model parameters are given in Table 4.5.

Table 4.5 Model parameters of the experimental system

Elastic modulus	2×10^{11} Pa
Poisson ratio	0.3
Density	7800 kg/m^3
Payload mass	0.503 kg
Inertia of payload	200.332×10^{-6} kgm^2
Cable Diameter	Ø1.2 mm
Cross section	1.5x39.75 mm^2
Beam length (L_2)	402 mm
Rayleigh damping coefficients	η=0 and $\beta=7.64 \times 10^{-5}$
Motor rotational spring constant	K_{m1}=16000 Nm/rad
Control Motor rotational spring constant	K_{m2}=44690 Nm/rad
Number of finite elements	ne2=402
Time step	Δt=0.005 s

The natural frequencies obtained from both the experiments and simulations are given in Table 4.6. Before adding the cables to the model, the manipulator was actuated with three different motion profiles, and end point displacement results were compared to verify the model and obtain the damping ratio. The obtained results are shown in Figure 4.7.

Table 4.6 Obtained Natural Frequencies

	Experiment (Hz)	Modal Analysis (Hz)
Only Manipulator	7.5989	7.5872
With (.502 gr) Payload	2.3877	2.4030

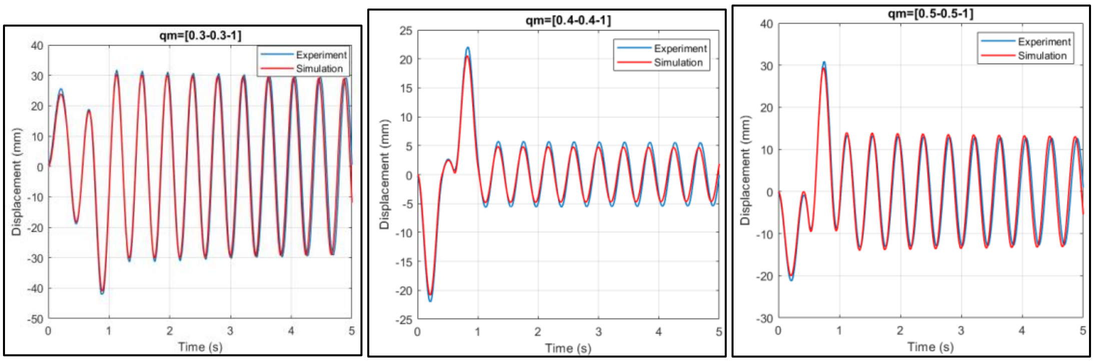

(a) (b) (c)

Figure 4.7 End point vibration of manipulator (only mass added) under different motion profiles

The results obtained from the transient analyses were sufficient for the verification of the model with and without the payload as shown in Figure 4.7 and Table 4.6.

Tensile tests on cable specimens were also performed in order to find the mechanical properties of cables and the data obtained are shown in Table 4.7.

Table 4.7 Tensile test result of cable specimens

	Elastic Modulus (N/mm^2)	Max Tensile Force (N)
Specimen1	82156.3	1241.79
Specimen2	65929.3	1185.73
Specimen3	85623.3	1219.48

However, adding the cables to the system and performing modal analysis was a complex task, because the existence of the cables adds more damping to the manipulator, while the first natural frequency of the manipulator when subjected to different motion profiles. In order to understand the behavior of the cables, the vibration results of the manipulator were observed under the given motion profiles.

The stiffness and damping effect of the cables were observed by comparing the vibration response of the manipulator under the same motion profile input for the models both with and without cables. The responses of the manipulator are shown in Figure 4.8. It was understood that the existence of the cables adds more stiffness and damping to the manipulator. In order to observe the behavior of the manipulator with cables, the vibration results of the manipulator were observed under the given motion profiles. The end point vibrations of the flexible manipulator with cables can be seen in Figure 4.9.

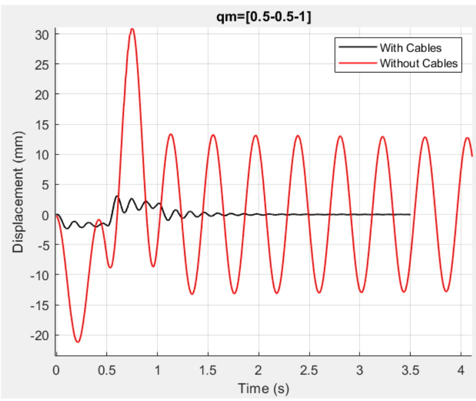

Figure 4.8. The experimental vibration response of the manipulator for $\mathbf{q}_m$=[0.5-0.5-1] for both with and without cables

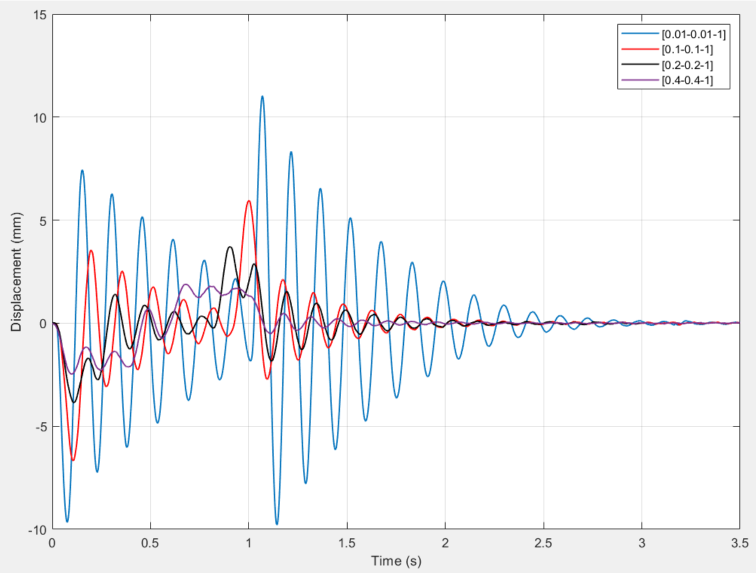

Figure 4.9 The end point vibrations of manipulator with cables (experimentally obtained data)

It is understood that the manipulator has different vibration frequencies under different motion profiles. The natural frequency obtained experimentally from the free vibration part of the motion can be seen in Table 4.8. The differences in frequency between the modal analyses and the fast Fourier transform, can be attributed to the fact that both cables are not effective at the same time on the stiffness matrix. The behavior of the system is compatible with the results obtained in section 4.2.

The adjustment of the initial tension of the cables needs to be measured then entered to the FE model. In this system the axial forces of the cables could not be obtained due to the lack of a measurement tool. The selection of the measurement tool and the revision required to add it to the experimental setup will be discussed in the next section.

Table 4.8 Obtained First Natural Frequencies under the different motion cases

	Trapezoidal Motion Cases / Obtained First Natural Frequencies						
Pretension	**[0.01-0.01-1]**	**[0.05-0.05-1]**	**[0.1-0.1-1]**	**[0.2-0.2-1]**	**[0.3-0.3-1]**	**[0.4-0.4-1]**	**[0.5-0.5-1]**
(Not Measured)	6.43 Hz	6.54 Hz	6.91 Hz	7.1 Hz	7.7 Hz	7.87 Hz	7.61 Hz

4.8 Controller Selection

An ADLIKN PCI 8253 motion control card was previously used to actuate the flexible manipulator using a prepared velocity input and time vector. However, this motion control card caused delays in real time closed loop control during the actuation of two motors at the same time. For this reason, the CODESYS system was selected to actuate the motors for closed loop control applications. CODESYS is more flexible than the ADLINK and can be used for many different applications.

In the system there are two motors. One of them was used to rotate the manipulator for a desired angle and the other one was used as a control actuator for suppressing the vibrations. Many different types of motion profiles were used in this thesis for passive control up to now. In this stage, trapezoidal motion profiles were preferred to actuate the main motor. For this reason, the motion vector was calculated in CODESYS. The motion profile parameters can be defined in the user interface as shown in Figure 4.10. Another switch was added to change the rotation direction. It is also possible to rotate the manipulator by using another velocity profile. Once the prepared velocity profile is read from a .txt file, it is stored in CODESYS and then the motor will rotate the manipulator according to the given input.

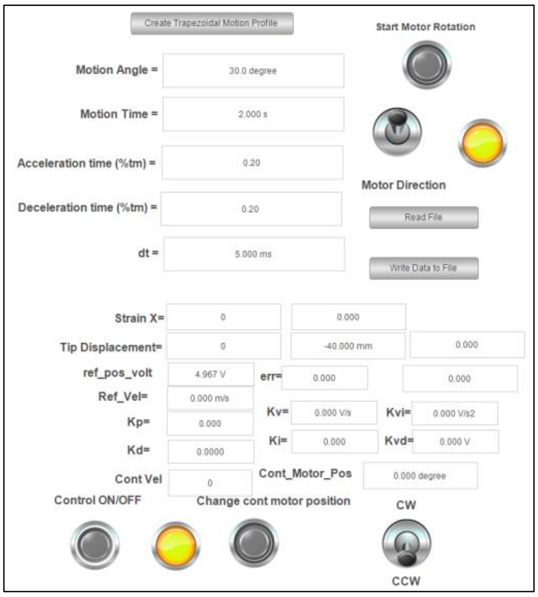

Figure 4.10 Created user interface in CODESYS

In the user interface, the reference value and control parameters (K_p, K_d, K_i) can be defined by the user. The dynamic strain gauge value or tip displacement which was measured with a laser displacement sensor Keyence LK-G157, can be observed by the user.

In order to control the motors and read the voltage from the strain gauge or laser displacement sensor, a digital and an analog output module, and an analog input module were used.

The servo motors can be actuated in different modes such as position, speed and torque control modes. In this case both motors were actuated in speed control mode. According to the used servo amplifier, the motor direction can be defined by connecting direction pins to another related pin as shown in Figure 4.11 (a). The motor velocity amplitudes can be set by using an analog voltage as shown in Figure 4.11 (a). For this reason, it was attempted to perform rotation switching by using relays which can be triggered by the digital output module. However, the relays cannot change the rotation direction during high speed triggers in the closed loop control. This problem was solved by using optocouplers. The optocouplers can make this switching every 1ms. When the optocoupler was triggered, the transistor in the optocoupler can switch immediately.

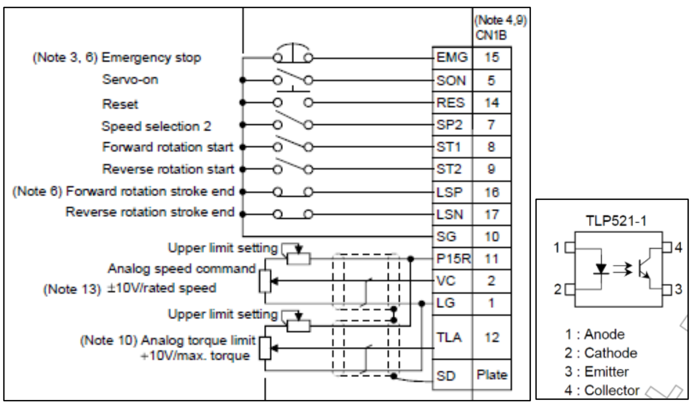

(a) (b)

Figure 4.11 (a) Servo amplifier control diagram (b) TLP521-1 optocoupler

4.9 Closed Loop Control Trials and Buckling Effects

The first experimental closed loop control trials were done by using strain feedback. It was attempted to suppress the residual vibrations under the given $\mathbf{q_m}$=[0.1-0.1-1] trapezoidal motion profile by using closed loop control. A proportional (K_p) controller was used. The closed loop control diagram is given in Figure 4.12.

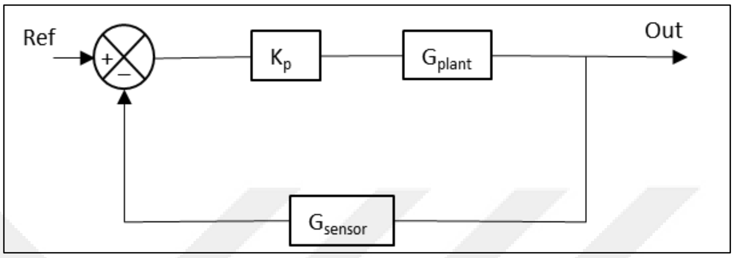

Figure 4.12 The closed loop control block diagram

The analog data read from the strain gauge at the stationary position was used as a reference, and after evaluation the error was multiplied with K_p, and the obtained value was sent to the servo amplifier as analog data. A time step of 5ms was chosen such that it did not exceed one-twentieth of the natural period.

After the verification, the closed loop control trials were performed for different K_p values and the results were shown in Figure 4.13. According to the results obtained, marginal closed loop control was achieved. When the K_p increases the overshoot also increased as expected. It was attempted to decrease the overshoot and settling time by adding K_d controller to the closed loop control. The main problem during the motion and control motor amplifier is also to try to keep and control the position of the motor. This one affects the control performance. For this problem the motor amplifier control parameters were changed, or another reducer was be used which has a higher reduction ratio than the current one.

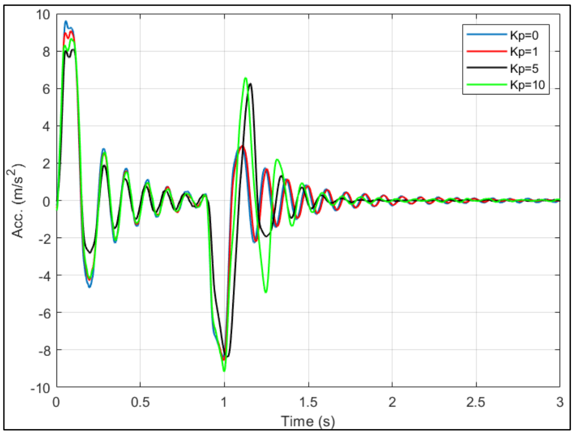

Figure 4.13 The closed loop control results for different K_p values

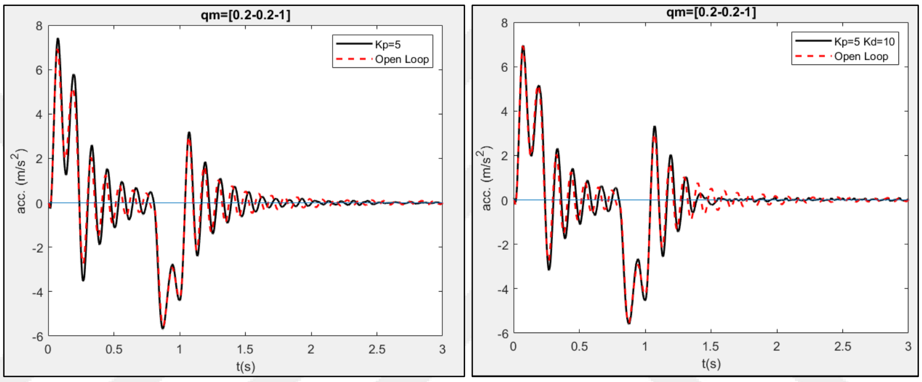

(a) (b)

Figure 4.14 (a) P controller results (b) PD controller results

Figure 4.14 shows the obtained acceleration output of the flexible manipulator, when the PD closed loop controller was used to suppress the residual vibrations. The flexible manipulator was actuated by the trapezoidal velocity motion profile $\mathbf{q_m}$=[0.2-0.2-1].

During the experiment it was observed from the tip displacement measurements, that the flexible manipulator deflected from its own axis when the cables were subjected to pretension. This happened due to buckling mechanism. The beam thickness which was 1.5mm was insufficient to prevent the buckling mechanism, a thicker beam should be used. The displacement measurements in the open loop experiments showed that the flexible manipulator with the pretension cables bent to one direction and vibrated at that axis as shown in Figure 4.15. The vibration results obtained from the displacement sensor for the rotated flexible manipulator to both clockwise and counterclockwise directions are shown in Figure 4.15.

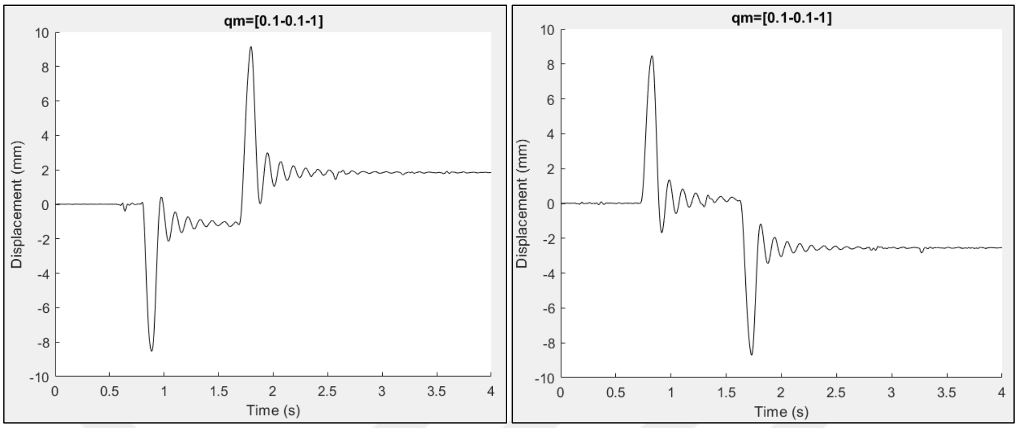

(a) (b)

Figure 4.15 (a) Clockwise (b) Counterclockwise rotated flexible manipulator tip displacement results

Therefor it was decided that the section dimension of the flexible beam would be changed to 4x40 mm^2. Simulation were performed, and the pretension of the cables was studied in order to make the natural frequency independent of the input velocity motion profiles.

The newly designed flexible manipulator dimensions were chosen 4x40x420 mm and a 1kg payload was added on the manipulator at 400 mm distance from the fixed rotation axis. When the pretension on the cables was as low as 5N, the natural frequency of the manipulator varied according to the given velocity motion profiles as it was shown in the previous part of this study. The pretension of the cables was increased up to 60N and the natural frequency of the manipulator was observed. The results of the simulations are given in Table 4.9.

Table 4.9 The effect of the pretension amount on the cables on the natural frequency

Pretension	**[0.1-0.1-1]**	**[0.2-0.2-1]**	**[0.3-0.3-1]**	**[0.4-0.4-1]**	**[0.5-0.5-1]**
30N	8.8477 Hz	8.8477 Hz	8.8477 Hz	8.8477 Hz	8.8477 Hz
60N	8.7891 Hz	8.7891 Hz	8.7891 Hz	8.7891 Hz	8.7891 Hz

Table 4.9 showed that the obtained first natural frequency in the residual vibration region was not dependent on the input velocity motion profile, since both cables remained strained for both 30N and 60N pretension values.

4.10 Revisions on the Experimental Setup

Two revisions were made to the experimental setup. The first revision was to add two mini load cells on the sliding upper part for the measurement of cable pretension amount. The added load cells are shown in Figure 4.16. Each added load cell can measure up to 50 kg loads. After this revision, the pretension axial load amount on the cables was measured indirectly. The dimensions of the flexible manipulator were also changed to 3.95x40x420 mm. A 1.25 kg payload was added on the manipulator at a 400 mm distance from the fixed rotation axis. When the pretension on the cables was as low as 5N, the natural frequency of the manipulator varied according to the given velocity motion profiles as shown in the previous part of this study. The pretension of the cables was increased up to 60N and the natural frequency of the manipulator were observed. The first natural frequency of the manipulator with cables under pretension obtained experimentally was 9.22 Hz.

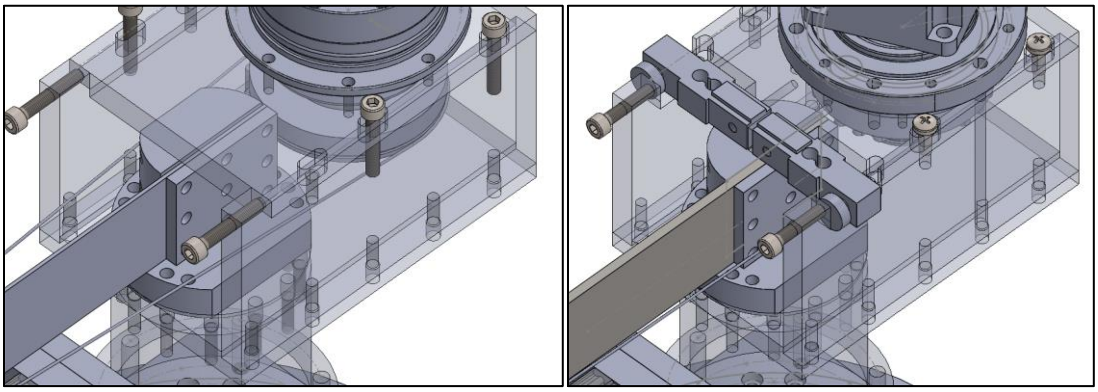

(a) (b)

Figure 4.16 (a) First design (b) Added mini load cells

After these revisions it was realized that the servo motor with the APEX reductor with a ratio of 1:10 cannot control its own position due the high inertia amount of the manipulator. This was observed when an impulse disturbance was applied to the manipulator, and the control motor tried to control its own position and became unstable. This problem was solved with another revision by changing the APEX 1:10 reductor with a harmonic drive reductor with a ratio of 1:80. The sliding upper part was revised again by increasing the diameter of the hole which the new reductor was mounted. The new four tapped holes were made to fix the harmonic reactor on the sliding upper part as shown in Figure 4.17.

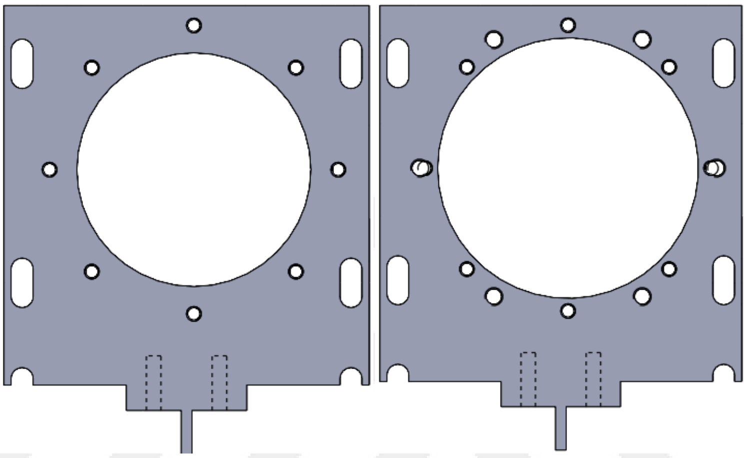

(a) (b)

Figure 4.17 Sliding upper part (a) After the first revision (b) After the second revision

After these revisions the first natural frequency of the manipulator with cables subjected to 60N pretension was experimentally determined to be 9.22 Hz. The natural frequency of the manipulator was high for the control motor to follow that frequency. A test was performed, a rigid link was connected to the output of the control motor reductor and the motor was actuated with an output function of $\theta(t)=0.1\sin(2\pi ft)$. The oscillation of the rigid link was measured with a laser displacement sensor. The output of the function $\theta(t)=0.1\sin(2\pi ft)$ was obtained in degrees. The frequency of the function was applied incrementally using 1 Hz steps up to 8 Hz. It was observed that the motor did not run properly when the frequency of the function is 8 Hz as shown in Figure 4.18 (b). The motor runs properly when frequency of the function has 6 Hz, giving adequate output both in terms of frequency and amplitude as shown in Figure 4.18 (a).

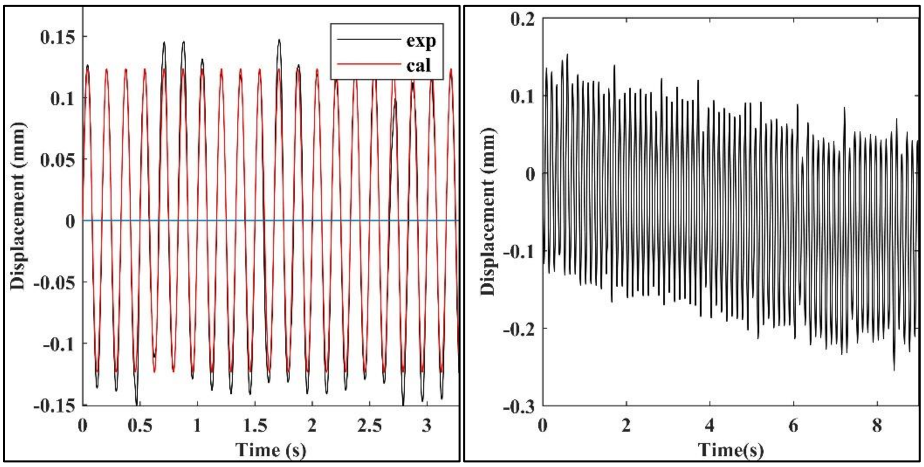

(a) (b)

Figure 4.18 (a) The 6 Hz oscillation (b)The 8 Hz oscillation of control motor

After the oscillation tests, it was decided to decrease the first natural frequency to around 6 Hz. The dimension of the flexible beam was changed to 3.95x40x450 mm, the payload increased up to 1.35 kg and the diameter of pulley which was connected to control motor reductor output was decreased to 30 mm.

4.11 Open and Closed Loop Control Results for Revised System

In this part of the study, the open loop and closed loop controls were performed both in simulation and experimentally for the last revised experimental setup. The last experimental setup model parameters are given in Table 4.10. The model dimensions are also given in Figure 4.19.

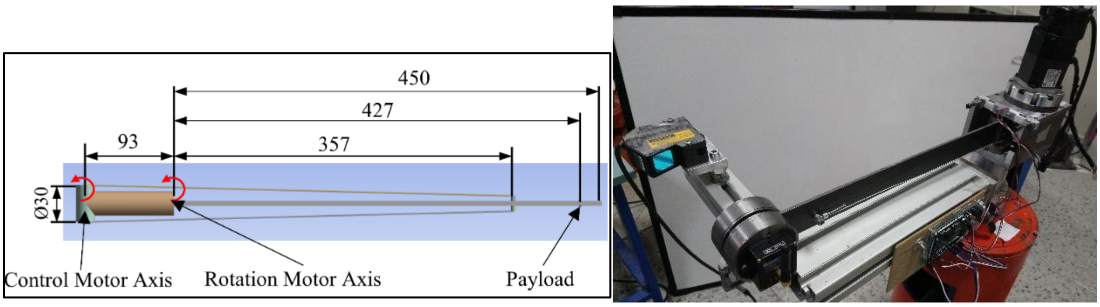

(a) (b)

Figure 4.19 (a) FE model and dimensions (b) Experimental setup

Table 4.10 Model parameters of the last revised experimental setup

Elastic modulus of manipulator	1.93×10^{11} Pa
Elastic modulus of cables	1.18×10^{11} Pa
Poisson ratio	0.3
Density of manipulator	7850 kg/m^3
Payload mass	1.35 kg
Inertia of payload	7.38×10^{-4} kgm^2
Cable diameter	Ø1.2 mm
Cross section	3.9x40 mm^2
Beam length	450 mm
Payload position from rotation axis	427 mm
Cable connection on manipulator from rotation axis	357 mm
Control motor center position from rotation axis	93 mm
Control pulley diameter	30 mm
Rayleigh damping coefficients	$\eta=0$ and $\beta=3 \times 10^{-4}$
Motor rotational spring constant	$K_{m1}=16000$ Nm/rad
Control Motor rotational spring constant	$K_{m2}=16000$ Nm/rad
Element size	1 mm
Time step	$\Delta t=0.001$ s

Trapezoidal motion profiles were used to actuate the manipulator. The manipulator was rotated by $\theta=30°$ in 1s. Symmetrical motion profiles were used. The acceleration time was selected from $0.2T_m$ to $0.5T_m$. The applied cable pretension amount was 105N. The open loop control results of the simulation were compared with the experimental results. The obtained results were shown in Figure 4.20. The obtained simulation results were fit well with the experimental results. The first natural frequency of the manipulator with the cables was measured to be 5.92 Hz.

The motion time was selected as 2 s for closed loop control experiments with the same rotation angle of $\theta=30°$ with $0.2T_m$ acceleration time. The velocity feedback was used for closed loop control by taking the derivative of the measured displacement data (André Preumont & Achkire, 1997; André Preumont et al., 2000; Warnitchai et al., 1993) The first closed loop block diagram that was used, is shown in Figure 4.21.

After the closed loop control results by using only the velocity feedback control for the residual part were obtained, it was observed that there was a position error as shown in Figure 4.22 (a). A second closed loop block diagram was used to eliminate the problem as shown in Figure 4.23. After using the block diagram with two feedback, shown in Figure 4.23, the new results were obtained as shown in Figure 4.22 (b) and (c). The RMS (root mean square) values of both open and closed loop control are given in Table 4.11. The closed loop control during the motion was also performed and the result is shown in Figure 4.22 (d). The RMS value of the closed loop control is given in Table 4.11.

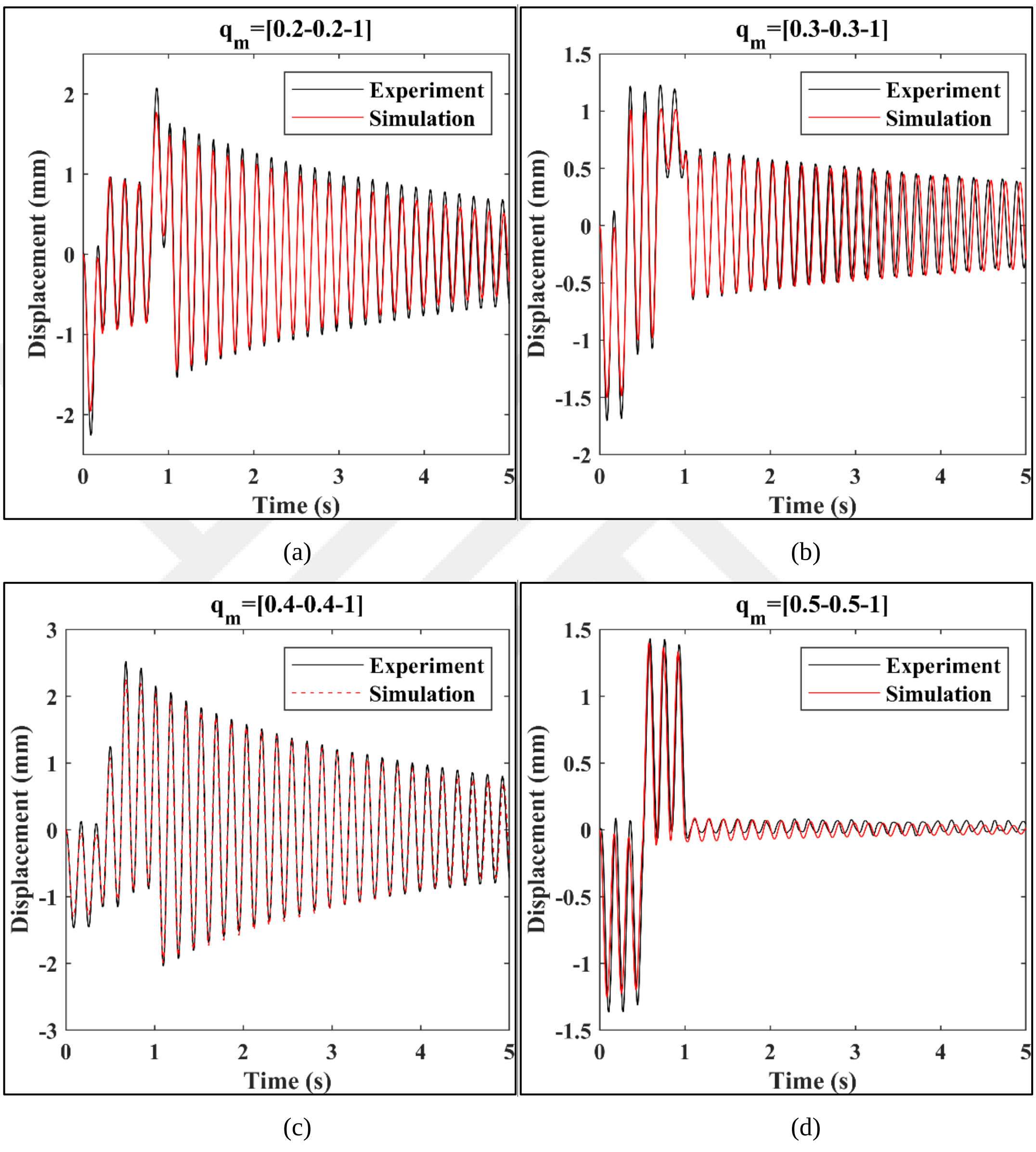

Figure 4.20 The obtained open loop results for both simulation and experiments

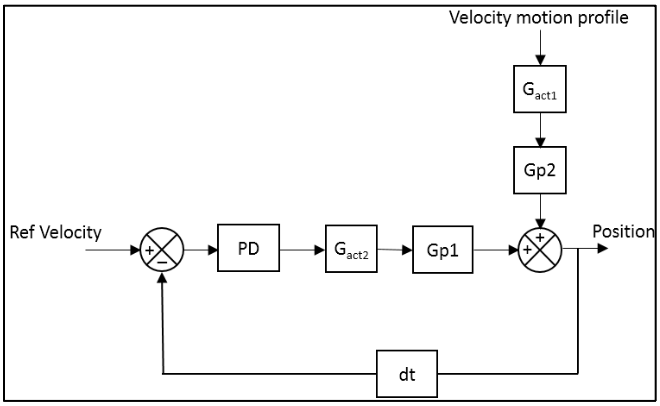

Figure 4.21 The used first closed loop control block diagram

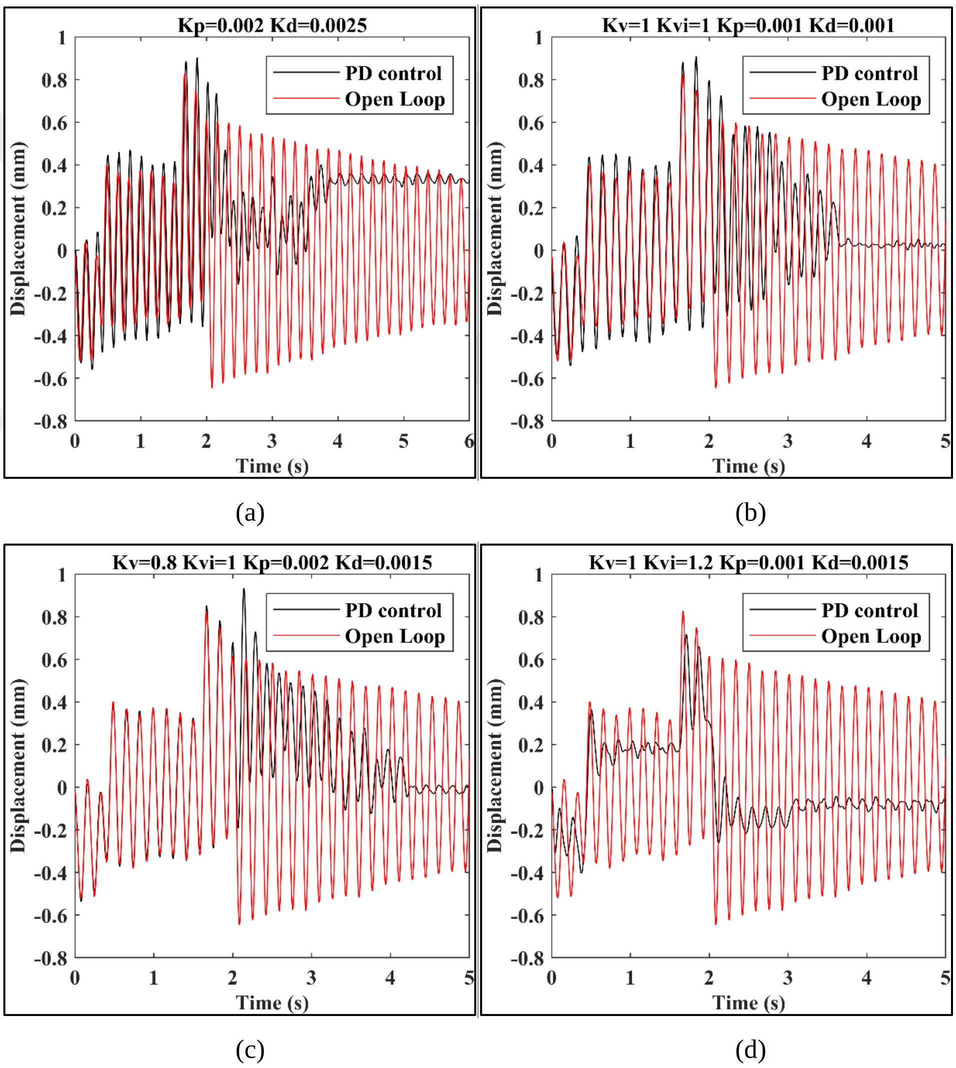

Figure 4.22 The closed loop control experimental results (a) only velocity feedback (b), (c) position and velocity feedback (d) position and velocity feedback during the motion

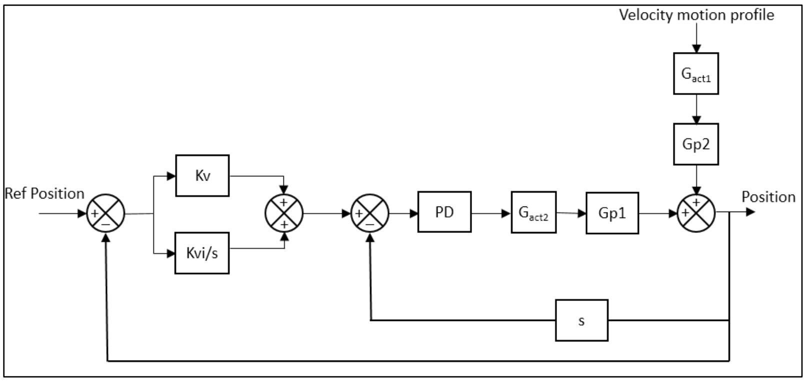

Figure 4.23 The used second closed loop control block diagram

Table 4.11 RMS values of some experimental both open and closed loop control

Control Parameter	Open loop (RMS)	Closed loop (RMS)
Kp=0.002 Kd=0.0025 (residual)	0.34	0.311
Kv=1 Kvi=1 Kp=0.001 Kd=0.001 (residual)	0.34	0.2803
Kv=0.8 Kvi=1 Kp=0.002 Kd=0.0015 (residual)	0.34	0.2789
Kv=1 Kvi=1.2 Kp=0.001 Kd=0.0015 (during the motion)	0.34	0.1965

The simulation results of the closed loop control for residual vibrations are given in Figure 4.24. The RMS values of the simulation closed loop control results are given in Table 4.12.

Table 4.12 RMS values of some simulation both open and closed loop control

Control Parameter	Open loop (RMS)	Closed loop (RMS)
Kp=1 Kd=6 (residual)	0.33	0.1954
Kp=1 Kd=6 (during motion)	0.33	0.0939
Kv=50 Kp=1 Kd=6 (during motion)	0.33	0.0324

The results of the experiment showed that closed loop control was achieved in terms of RMS values. However, the closed loop results were not very satisfactory and not robust. The results of the simulations were more satisfactory than the experiments. The reason is that taking numerical derivatives during the experiment, caused unwanted sudden changes during the motion. The acceleration feedback can be used to avoid this problem by taking numerical integration to achieve velocity feedback for the next studies. However, in the simulation there was no such type of noise. The experimental open loop control results fit well with the simulation results which shows that the Gp2, which is the transfer function between the output position and velocity motion profile input, was modeled correctly in the simulation. However, the same fit between the experiment and simulation could not be achieved for the closed loop control. The reason behind this is that the model of the control motor transfer function could not be implemented in ANSYS. Therefore, the Gp1, which is the transfer function between the output position and control motor velocity input, was not modeled correctly in the simulation. However, the experimental closed loop control was partially successful.

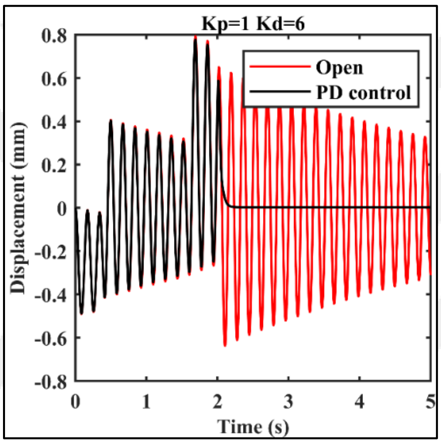

(a)

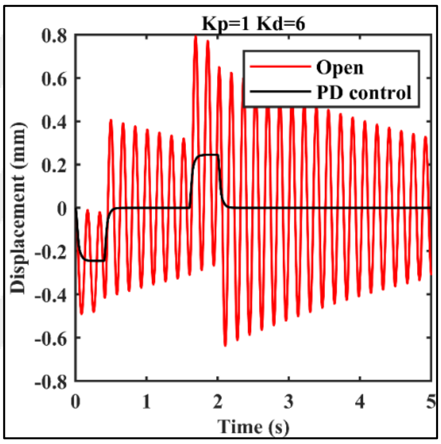

(b)

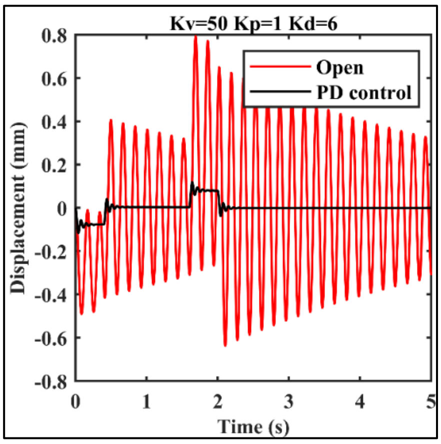

(c)

Figure 4.24 The closed loop simulation results (a) only velocity feedback (b), (c) position and velocity feedback during the motion

4.12 Conclusions

In this part the FE model of the flexible manipulator was created. The open and closed loop simulations were performed in order to design an experimental setup. An experimental setup was designed, and the required revisions were done due the problems encountered. A pretension measurement system was also added to measure the axial pretensions on the cables. The effect of pretension of the cables on the natural frequency of the flexible manipulator was also observed. Open and closed loop control was performed after the last revised experimental setup. The results were given and explained in terms of RMS values. However, the experimental closed loop control results were not very satisfactory and not robust. The results of the simulations were more satisfactory than the results of the experiments. The reason is that the velocity feedback was calculated by taking numerical derivatives of the position. This caused unwanted sudden changes during the motion. The acceleration feedback can be used to avoid this problem by taking numerical integration to achieve velocity feedback in future studies. Other types of controllers can also be used to obtain much robust control, such as nonlinear controllers, positive position feedback controller etc. The experimental open loop control results fit well with the simulation results which shows that the Gp2, which is the transfer function between the output position and velocity motion profile input, was modeled correctly in the simulation. However, the same fit between the experiment and simulation results could not be achieved for the closed loop control. The reason behind this is that the model of the control motor transfer function could not be implemented in ANSYS. Therefore, the Gp1, which is the transfer function between the output position and control motor velocity input, was not modeled correctly in the simulation. However, experimental closed loop control was partially successful.

CHAPTER FIVE
CONCLUSIONS

In this study both passive and active vibration control of the flexible manipulators was studied. Firstly, the effect of the time parameters of both 3rd order polynomial S-curve and trapezoidal motion on the transient and residual vibrations of a flexible manipulator were investigated. This investigation was done by using ANSYS simulations and Newmark method. The FE model of the manipulator was created in MATLAB and the transient response of the flexible manipulator under a given velocity motion profile was calculated by using the Newmark method. When the 3rd order polynomial S-curve motion profile time parameters were defined as integer multiples of the fundamental natural period of the flexible manipulator, the residual vibrations were reduced effectively. The comparison between the S-curve motion profile and trapezoidal motion profile results were also investigated for different motion cases. It was observed that the residual and transient vibrations amplitudes of the manipulator under the S-curve motion profile were less than trapezoidal ones, even if they reached the same maximum velocity, while the S-curve motion profiles reached higher acceleration values than the trapezoidal ones. It was observed that the presence of T_2 which is an S-curve motion time parameter caused smaller maximum transient vibration amplitudes, when compared to the results of a trapezoidal motion profile which have the same acceleration time. In the case of the S-curve motion profiles, it was observed that the selection of T_4 as either zero or any multiple of the first natural period of the flexible manipulator did not affect the residual vibration amplitudes. However, for the trapezoidal motion profiles the selection of T_{cons} as an integer multiple of the first natural period of the flexible manipulator is important to reduce the residual vibration amplitudes. In order to obtain minimum residual vibration amplitudes under the trapezoidal velocity motion profile, all the time parameters should be selected as integer multiples of the fundamental natural period of the flexible manipulator. On the other hand, all the S-curve motion profile time parameters besides T_4 should be selected as integer multiples of the first natural period of the manipulator. However, the acceleration time should be selected long if possible, for both the S-curve and trapezoidal motion profiles in order to reduce transient vibration amplitudes.

In order to obtain the minimum transient vibration amplitudes for the S-curve motion profiles, T_1 should be at least 2t1h and T_2 should be as long as possible depending on T_m. The T_{acc} and T_{dec} times of the trapezoidal motion profiles should be selected as long as possible and T_{cons} should be selected as short as possible in order to obtain less transient vibration amplitudes.

The second part of the study presents the effect of three different, seven segment velocity motion profiles on the end point transient and residual vibrations of a flexible manipulator that were experimentally and numerically investigated. These motion profiles were the 3rd order polynomial S-curve and two different trigonometric (harmonic and pure sinusoidal) S-curve motion profiles. The experimental results were compared with the transient analysis results obtained with ANSYS. The effect of time parameters of all motion profiles on endpoint vibrations was investigated by comparing them in terms of amplitudes.

It was shown that the selection of the time parameters as integer multiples of the fundamental period is effective in reducing residual vibration amplitudes to almost zero for 3rd order polynomial S-curve motion profiles. The time parameters of the trigonometric profiles (harmonic and pure sinusoidal) should be selected as half integer multiples of the fundamental period of the manipulator to obtain almost zero residual vibrations.

The sensitivity of all motion profiles to any measurement error in the range of 0% to 4% during the measurement of the natural frequency of the manipulator was also shown. The polynomial S-curve motion profile results were less sensitive than sinusoidal motion profiles for motion case $\mathbf{q}_m$=[2t1h, 4t1h, 2t1h, 20t1h], while sinusoidal ones caused less error than polynomial motion profile for motion case $\mathbf{q}_m$=[3t1h, 3t1h, 3t1h, 21t1h]. For this reason, as a precaution against a possible measurement error, if T_1 and T_m were selected as 2t1h and (2n)t1h ($n \in \mathbb{N}$) respectively, the polynomial S-curve motion profiles should be preferred. Otherwise, if T_1 and T_m were selected as 3t1h and (2n+1)t1h ($n \in \mathbb{N}$) respectively, the pure sinusoidal motion profile should be preferred.

Finally, the active vibration control of the flexible manipulator was studied. The FE model of the flexible manipulator was created. The open and closed loop simulations were performed in order to design an experimental setup. An experimental setup was designed, and the required revision were done due the encountered problems. The pretension measurement system was also added to measure the axial pretension on the cables. The effect of the pretension of the cables on the natural frequency of the flexible manipulator was also observed. The open and closed loop control were performed on the last revised experimental setup. The obtained results were given and explained in terms of RMS values. However, the experimental closed loop control results were not very satisfactory and not robust. The obtained results of the simulations were more satisfactory than the experiments. The reason is that the velocity feedback was calculated by taking numerical derivatives of the position. This caused unwanted sudden changes during the motion. The acceleration feedback can be used to avoid this problem by taking numerical integration to achieve velocity feedback for the future studies. Other types of controllers, such as nonlinear controllers, positive position feedback controller etc., can be used to obtain a more robust control. The experimental open loop control results fit well with the simulation results which shows that the relationship between the output position and velocity motion profile input was modeled correctly in the simulation. However, the same fit between the experiment and simulation could not be achieved for the closed loop control. The reason is that the model of the control motor transfer function could not be implemented in ANSYS. Therefore, the relationship between the output position and control motor velocity input was not modeled correctly in the simulation. However, experimental closed loop control was partially successful.

REFERENCES

Achkire, Y., Bossens, F., & Preumont, A. (1998). Active damping and flutter control of cable-stayed bridges. *Journal of Wind Engineering and Industrial Aerodynamics, 74*, 913-921.

Achkire, Y., & Preumont, A. (1996). Active tendon control of cable‐stayed bridges. *Earthquake engineering & structural dynamics, 25*(6), 585-597.

Akdağ, M., & Şen, H. (2021). S-curve Motion Profile Design for Vibration Control of Single Link Flexible Manipulator. *Dokuz Eylül Üniversitesi Mühendislik Fakültesi Fen ve Mühendislik Dergisi, 23*(68), 661-676.

Akdağ, M., & Şen, H. (2023). Investigation of Performance and Sensitivity of S-Curve Motion Profiles on Reduction in Flexible Manipulator Vibrations. *Arabian Journal for Science and Engineering*, 1-14.

Ankarali, A., & Diken, H. (1997). Vibration Control of an Elastic Manipulator Link. *Journal of Sound and Vibration, 204*(1), 162-170. doi:10.1006/jsvi.1996.0897

Bathe, K. (2014). *Finite Element Procedures* (2nd ed.): USA: Prentice Hall, Person Education, Inc.

Benosman, M., & Le Vey, G. (2004). Control of Flexible Manipulators: A survey. *Robotica, 22*(5), 533-545. doi:10.1017/S0263574703005642

Bernzen, W. (1999). Active vibration control of flexible robots using virtual spring-damper systems. *Journal of intelligent and robotic systems, 24*(1), 69-88.

Boryga, M., & Graboś, A. (2009). Planning of Manipulator Motion Trajectory with Higher-Degree Polynomials Use. *Mechanism and machine theory, 44*(7), 1400-1419. doi:10.1016/j.mechmachtheory.2008.11.003

Bossens, F., & Preumont, A. (2001). Active tendon control of cable‐stayed bridges: a large‐scale demonstration. *Earthquake engineering & structural dynamics, 30*(7), 961-979.

Castain, R. H., & Paul, R. P. (1984). An on-line dynamic trajectory generator. *The International Journal of Robotics Research, 3*(1), 68-72. doi:10.1177/027836498400300106

Diken, H., & Alghamdi, A. (2003). Residual vibration response spectra for a servomotor-driven flexible beam. *Proceedings of the Institution of Mechanical Engineers, Part C: Journal of Mechanical Engineering Science, 217*(5), 577-583. doi:10.1243/095440603765226867

Dubay, R., Hassan, M., Li, C., & Charest, M. (2014). Finite element based model predictive control for active vibration suppression of a one-link flexible manipulator. *Isa Transactions, 53*(5), 1609-1619.

Dwivedy, S. K., & Eberhard, P. (2006). Dynamic analysis of flexible manipulators, a literature review. *Mechanism and machine theory, 41*(7), 749-777. doi:10.1016/j.mechmachtheory.2006.01.014

Fang, Y., Hu, J., Liu, W., Shao, Q., Qi, J., & Peng, Y. (2019). Smooth and time-optimal S-curve trajectory planning for automated robots and machines. *Mechanism and machine theory, 137*, 127-153. doi:10.1016/j.mechmachtheory.2019.03.019

Gao, Y., Wang, F.-Y., Zhao, Z.-Q., & Xiao, Z.-Q. (2012). *Flexible manipulators: modeling, analysis and optimum design*: Academic Press.

Ha, C.-W., & Lee, D. (2017). Analysis of embedded prefilters in motion profiles. *IEEE Transactions on Industrial Electronics, 65*(2), 1481-1489.

Hassan, M., Dubay, R., Li, C., & Wang, R. (2007). Active vibration control of a flexible one-link manipulator using a multivariable predictive controller. *Mechatronics, 17*(6), 311-323.

Hillsley, K. L., & Yurkovich, S. (1993). Vibration control of a two-link flexible robot arm. *Dynamics and Control, 3*(3), 261-280.

Ilman, M. M., Yavuz, Ş., Karagülle, H., & Uysal, A. (2022). Hybrid vibration control of an industrial CFRP composite robot-manipulator system based on reduced order model. *Simulation Modelling Practice and Theory, 115*, 102456.

Jnifene, A. (2007). Active vibration control of flexible structures using delayed position feedback. *Systems & control letters, 56*(3), 215-222.

Jnifene, A., & Andrews, W. (2005). Experimental study on active vibration control of a single-link flexible manipulator using tools of fuzzy logic and neural networks. *IEEE transactions on instrumentation and measurement, 54*(3), 1200-1208.

Karagülle, H., Malgaca, L., Dirilmiş, M., Akdağ, M., & Yavuz, Ş. (2017). Vibration control of a two-link flexible manipulator. *Journal of Vibration and Control, 23*(12), 2023-2034. doi:10.1177/1077546315607694

Kim, B., Yoo, H. H., & Chung, J. (2017). Robust Motion Profiles for the Residual Vibration Reduction of an Undamped System. *Journal of Mechanical Science and Technology, 31*(10), 4647-4656. doi:10.1007/s12206-017-0911-9

Kim, J., & Croft, E. A. (2018). Preshaping input trajectories of industrial robots for vibration suppression. *Robotics and Computer-Integrated Manufacturing, 54*, 35-44.

Lambrechts, P., Boerlage, M., & Steinbuch, M. (2005). Trajectory planning and feedforward design for electromechanical motion systems. *Control Engineering Practice, 13*(2), 145-157. doi:10.1016/j.conengprac.2004.02.010

Li, H., Gong, Z., Lin, W., & Lippa, T. (2006, 16-18 Aug.). *A New Motion Control Approach for Jerk and Transient Vibration Suppression.* Paper presented at the 2006 4th IEEE International Conference on Industrial Informatics, Singapore.

Li, H., Le, M., Gong, Z., & Lin, W. (2009). Motion profile design to reduce residual vibration of high-speed positioning stages. *IEEE/ASME Transactions On Mechatronics, 14*(2), 264-269. doi:10.1109/TMECH.2008.2012160

Liu, C., & Chen, Y. (2018). Combined S-curve feedrate profiling and input shaping for glass substrate transfer robot vibration suppression. *Industrial Robot: the international journal of robotics research and application, 45*(4), 549-560. doi:10.1108/ir-11-2017-0201

Liu, S. (2002, 3-5 July). *An on-line reference-trajectory generator for smooth motion of impulse-controlled industrial manipulators.* Paper presented at the 7th International Workshop on Advanced Motion Control. Proceedings (Cat. No. 02TH8623), Maribor, Slovenia.

Liu, X., Zhang, H., Lv, L., Peng, F., & Cai, G. (2018). Vibration control of a membrane antenna structure using cable actuators. *Journal of the Franklin Institute, 355*(5), 2424-2435.

Lu, E., Li, W., Yang, X., Wang, Y., & Liu, Y. (2018). Optimal placement and active vibration control for piezoelectric smart flexible manipulators using modal H 2 norm. *Journal of Intelligent Material Systems and Structures, 29*(11), 2333-2343.

Lu, T.-C., & Chen, S.-L. (2016). Genetic algorithm-based S-curve acceleration and deceleration for five-axis machine tools. *The International Journal of Advanced Manufacturing Technology, 87*(1-4), 219-232. doi:10.1007/s00170-016-8464-0

Malgaca, L., Yavuz, Ş., Akdağ, M., & Karagülle, H. (2016). Residual vibration control of a single-link flexible curved manipulator. *Simulation Modelling Practice and Theory, 67*, 155-170. doi:10.1016/j.simpat.2016.06.007

Meckl, P. H., & Arestides, P. B. (1998, 26-26 June). *Optimized s-curve motion profiles for minimum residual vibration.* Paper presented at the Proceedings of the 1998 American Control Conference. ACC (IEEE Cat. No. 98CH36207), Philadelphia, PA, USA.

Mohamed, Z., & Tokhi, M. O. (2004). Command shaping techniques for vibration control of a flexible robot manipulator. *Mechatronics, 14*(1), 69-90.

Mu, H., Zhou, Y., Yan, S., & Han, A. (2008). Third-order trajectory planning for high accuracy point-to-point motion. *Frontiers of Electrical and Electronic Engineering in China, 4*(1), 83-87. doi:10.1007/s11460-009-0017-y

Newmark, N. M. (1959). A method of computation for structural dynamics. *Journal of the engineering mechanics division, 85*(3), 67-94. doi:10.1061/JMCEA3.0000098

Nguyen, K. D., Ng, T.-C., & Chen, I.-M. (2008). On Algorithms for Planning S-curve Motion Profiles. *International Journal of Advanced Robotic Systems, 5*(1), 11. doi:10.5772/5652

Preumont, A., & Achkire, Y. (1997). Active damping of structures with guy cables. *Journal of guidance, control, and dynamics, 20*(2), 320-326.

Preumont, A., Achkire, Y., & Bossens, F. (2000). Active tendon control of large trusses. *AIAA journal, 38*(3), 493-498.

Preumont, A., & Bossens, F. (2000). Active tendon control of vibration of truss structures: Theory and experiments. *Journal of Intelligent Material Systems and Structures, 11*(2), 91-99.

Preumont, A., Voltan, M., Sangiovanni, A., Mokrani, B., & Alaluf, D. (2016). Active tendon control of suspension bridges. *Smart Struct. Syst, 18*(1), 31-52.

Qiu, Z.-c., Li, C., & Zhang, X.-m. (2019). Experimental study on active vibration control for a kind of two-link flexible manipulator. *Mechanical Systems and Signal Processing, 118*, 623-644.

Rodellar, J., Mañosa, V., & Monroy, C. (2002). An active tendon control scheme for cable‐stayed bridges with model uncertainties and seismic excitation. *Journal of Structural Control, 9*(1), 75-94.

Sayahkarajy, M., Mohamed, Z., & Mohd Faudzi, A. A. (2016). Review of modelling and control of flexible-link manipulators. *Proceedings of the Institution of Mechanical Engineers, Part I: Journal of Systems and Control Engineering, 230*(8), 861-873. doi:10.1177/0959651816642099

Singer, N. C., & Seering, W. P. (1990). Preshaping command inputs to reduce system vibration.

Subedi, D., Tyapin, I., & Hovland, G. (2020). Review on modeling and control of flexible link manipulators.

Thomsen, D. K., Søe-Knudsen, R., Balling, O., & Zhang, X. (2021). Vibration control of industrial robot arms by multi-mode time-varying input shaping. *Mechanism and machine theory, 155*, 104072.

Tzes, A., & Yurkovich, S. (1993). An adaptive input shaping control scheme for vibration suppression in slewing flexible structures. *IEEE Transactions on Control Systems Technology*, *1*(2), 114-121.

Tzou, H. (1989). Integrated distributed sensing and active vibration suppression of flexible manipulators using distributed piezoelectrics. *Journal of Robotic Systems*, *6*(6), 745-767.

W. T. Thomson, M. D. D. (1988). *Theory of Vibration with Applications* (3rd ed.). Englewood Cliffs: Prentice-Hall.

Warnitchai, P., Fujino, Y., Pacheco, B. M., & Agret, R. (1993). An experimental study on active tendon control of cable‐stayed bridges. *Earthquake engineering & structural dynamics*, *22*(2), 93-111.

Wei, J.-j., Qiu, Z.-c., Han, J.-d., & Wang, Y.-c. (2010). Experimental comparison research on active vibration control for flexible piezoelectric manipulator using fuzzy controller. *Journal of intelligent and robotic systems*, *59*, 31-56.

Yatim, H., & Mat Darus, I. (2014). Self-tuning active vibration controller using particle swarm optimization for flexible manipulator system. *WSEAS Transactions on Systems and Control*, *9*(1), 55-66.

Yavuz, Ş., Malgaca, L., & Karagülle, H. (2016). Vibration control of a single-link flexible composite manipulator. *Composite Structures*, *140*, 684-691. doi:10.1016/j.compstruct.2016.01.037